

Spotlight Selection | Environmental Microbiology | Full-Length Text

# Lipid hydrogen isotope compositions primarily reflect growth water in the model archaeon *Sulfolobus acidocaldarius*

Carolynn M. Harris,<sup>1</sup> Sebastian Kopf,<sup>2</sup> Jeemin H. Rhim,<sup>1,3</sup> Alec Cobban,<sup>1</sup> Felix J. Elling,<sup>4,5</sup> Xiahong Feng,<sup>1</sup> Jamie McFarlin,<sup>2,6</sup> Yuki Weber,<sup>4</sup> Yujiao Zhang,<sup>1</sup> Alice Zhou,<sup>1</sup> Harpreet Bather,<sup>2</sup> Ann Pearson,<sup>4</sup> William D. Leavitt<sup>1,7</sup>**AUTHOR AFFILIATIONS** See affiliation list on p. 17.

**ABSTRACT** The stable hydrogen isotope composition ( $\delta^2\text{H}$ ) of lipid biomarkers can track environmental processes and remain stable over geologically relevant time scales, enabling studies of past climate, hydrology, and ecology. Most research has focused on lipids from the domain Eukarya (e.g., plant waxes, long-chain alkanes), and the potential of prokaryotic lipid biomarkers from the domain Archaea to offer unique insights into environments not captured by eukaryotic lipids remains unclear. Here, we investigate the H-isotope composition of biphytanes in *Sulfolobus acidocaldarius*, a model thermoacidophile and obligate heterotroph. We conducted a series of experiments that varied temperature, pH, shaking rate, electron acceptor availability, or electron donor flux. From these experiments, we quantified the lipid/water H-isotope fractionation ( $^2\varepsilon_{L/W}$ ) values for core biphytane chains derived from tetraether lipids. The  $^2\varepsilon_{L/W}$  values are consistently negative ( $-230\text{‰}$  to  $-180\text{‰}$ ) and are relatively invariant across all experiments despite a 20-fold change in doubling times and a twofold change in lipid cyclization. The magnitude and relative invariance of  $^2\varepsilon_{L/W}$  values are consistent with studies on other heterotrophic archaea and suggest archaeal lipids may be faithful recorders of the  $\delta^2\text{H}$  composition of growth water. Our study highlights the potential of archaeal lipid  $\delta^2\text{H}$  values as a hydrological proxy, offering new insights into environments where traditional proxies, such as plant-derived lipids, are not available, including extreme environments and extraterrestrial settings.

**IMPORTANCE** Reconstructing past climates is crucial for understanding Earth's environmental history and its responses to changing conditions. This study examines *Sulfolobus acidocaldarius*, a thermoacidophilic archaeon that thrives in extreme environments like hot springs. These microorganisms incorporate hydrogen water in the growth environment into membrane lipids, creating hydrogen isotope signatures that can reflect hydroclimate conditions. Our findings show that these hydrogen isotope ratios remain consistent even under varying temperatures, pH, oxygen levels, and electron donor fluxes, indicating a stable fractionation between lipids and water. This invariance suggests that *S. acidocaldarius* lipids could serve as a robust proxy for reconstructing ancient water H-isotope values, especially in extreme environments where traditional proxies, such as plant waxes, are absent. This research has broader implications for planetary-scale reconstructions, including potential applications in studying past climates on other planets, such as Mars, where similar microorganisms may have existed in hydrothermal conditions.

**KEYWORDS** archaeal lipids, tetraether lipids, GDGTs, biphytanes, hydrogen isotope, biomarkers

The relative abundances of hydrogen isotopes ( $^2\text{H}/^1\text{H}$ ) in water are set by physical, hydrological, and climatic factors (1, 2). Certain biomolecules incorporate these

**Editor** Betül Kaçar, University of Wisconsin-Madison, Madison, Wisconsin, USA

Address correspondence to Carolynn M. Harris, carolynn.m.harris.gr@dartmouth.edu.

The authors declare no conflict of interest.

See the funding table on p. 17.

This article was handled by Betül Kaçar, who acted as a Guest Editor in consultation with the Editor in Chief, Gemma Reguera.

**Received** 21 October 2024

**Accepted** 28 January 2025

**Published** 25 March 2025

Copyright © 2025 Harris et al. This is an open-access article distributed under the terms of the [Creative Commons Attribution 4.0 International license](https://creativecommons.org/licenses/by/4.0/).

isotopes with a consistent offset (fractionation) relative to water, preserving a record of the isotopic composition ( $\delta^2\text{H}$  values) of the water present during growth (3). Some lipids can retain their original H-isotope composition for up to  $10^8$  years and lipid hydrogen isotope compositions have been used to study hydrologic and environmental change over millennia to millions of years, dating as far back as the Paleoproterozoic (4–6). Most studies of biomarker H-isotope composition focus on lipids from photoautotrophic organisms (e.g., plant wax *n*-alkanes) or chemoautotrophic and heterotrophic bacteria (e.g., fatty acids) (3, 7–9) and the H-isotope compositions recorded in lipids from the Archaea are comparatively poorly understood. A small, but growing, body of literature, however, has begun to address this gap (10–15). Understanding the extent to which the  $\delta^2\text{H}$  value of archaeal lipids records the  $\delta^2\text{H}$  value of growth water requires a deeper examination of how environmental conditions impact this signal. A comprehensive investigation of the physicochemical factors affecting H-isotope fractionation between archaeal lipids and water ( $^2\varepsilon_{L/W}$ ) is essential for employing archaeal lipid  $\delta^2\text{H}$  composition as a proxy for the  $\delta^2\text{H}$  composition of environmental water over space and time.

The  $^2\varepsilon_{L/W}$  value for a biomolecule integrates both the composition of source water and the net biosynthetic fractionations resulting from the specific pathways used during lipid biosynthesis. Reported  $^2\varepsilon_{L/W}$  values vary widely among domains of life. In phototrophic Eukaryotes (e.g., plants and algae),  $^2\varepsilon_{L/W}$  values of waxes (e.g., *n*-alkanes) are consistently negative, ranging from  $-150\text{‰}$  to  $-50\text{‰}$  (8, 16). It is important to understand the causes of this variability when applying lipid  $\delta^2\text{H}$  values to reconstruct water  $\delta^2\text{H}$  values. Net biosynthetic fractionation is generally consistent across taxa, though genetic factors introduce some variance (17–22). Environmental factors such as temperature, salinity, light availability, and  $\text{CO}_2$  concentration, also influence  $^2\varepsilon_{L/W}$  values, possibly via their impact on growth and biosynthesis rates (16, 23–28). These effects are well-characterized in plants, and to a lesser extent in algae, and can be accounted for when the  $\delta^2\text{H}$  values of plant waxes are used to reconstruct past hydroclimate (8, 29, 30).

In contrast to the coherent magnitude and direction of  $^2\varepsilon_{L/W}$  values observed from phototrophic eukaryotes, the  $^2\varepsilon_{L/W}$  of bacterial fatty acids varies widely in both direction and magnitude ( $-400\text{‰}$  to  $+300\text{‰}$ ) (31–38). Bacteria that use different central energy metabolisms (e.g., chemoautotrophy, photoautotrophy, or heterotrophy) exhibit distinct ranges of  $^2\varepsilon_{L/W}$  values, which has been attributed to differences in metabolic pathways and the substrate used for growth (e.g., simple sugars vs tricarboxylic acid [TCA] cycle intermediates). A recent study suggests that variations in  $^2\varepsilon_{L/W}$  values from aerobic heterotrophic bacteria are explained by energy fluxes through the intracellular hydride carriers  $\text{NADP}^+$  and  $\text{NADPH}$  (38). Given this metabolism-dependent heterogeneity, the  $\delta^2\text{H}$  values of bacterial lipids in sediment records may have more utility as proxies for the energetic state of past microbial metabolisms (33, 36, 38).

Lipid-water  $^2\text{H}$ -fractionation from the domain Archaea has been understudied to date. From what we do know,  $^2\varepsilon_{L/W}$  values have been reported for diether lipids (archaeol) in a mesophilic halophile (11) and a methanogen (13), tetraether-derived biphytanes in three thermoacidophiles and one thermomesophile (10, 15), and one aerobic marine chemoautotroph (14), and whole tetraethers or tetraether-derived biphytanes in several environmental sediment samples (10, 12). The observed  $^2\varepsilon_{L/W}$  values for these archaeal lipids are uniformly negative (i.e.,  $-300\text{‰}$  to  $-150\text{‰}$ ) and similar in magnitude to those reported for isoprenoid lipids produced by eukaryotic phototrophs (e.g.,  $\text{C}_{15}$  and  $\text{C}_{30}$  isoprenoids) (3, 25).

Our understanding of the factors controlling the H-isotope compositions of archaeal lipids is less developed than for the Eukarya and Bacteria. Recent experiments demonstrate that  $^2\varepsilon_{L/W}$  is nearly constant over a range of growth rates in a marine autotroph (*Nitrosopumilus maritimus* [14]) and that the impacts of carbon metabolism and growth phase on  $^2\varepsilon_{L/W}$  are minor (*Archaeoglobus fulgidus* [15]). This relative invariance in  $^2\varepsilon_{L/W}$  values is perhaps surprising considering the taxonomic and metabolic diversity

of the investigated Archaea. The impact of environmental factors on this fractionation, however, has only been investigated within a single archaeal strain (*Haloarcula marismortui* [11]). Further investigation of the effects of multiple environmental factors on  $^{2}\epsilon_{L/W}$  in Archaea is crucial, particularly since many archaea are adapted to extreme environments that can experience both rapid and large changes to physicochemical conditions (39).

Isoprenoid glycerol dibiphytanyl glycerol tetraethers (iGDGTs) are archaeal lipids with particular relevance to paleoenvironmental reconstructions (40). These tetraethers are structurally diagnostic, diagenetically robust, and routinely analyzed for paleoclimate reconstruction based on the relative abundances of specific structural moieties (40–42). Archaea can synthesize a unique series of iGDGTs that contain from zero to eight cyclopentane rings (e.g., iGDGT-0 through iGDGT-8), though the most highly ringed moieties (iGDGT-7 and -8) have only been recovered from hydrothermal spring environments (43). Members of the Thaumarchaeota phyla can also produce crenarchaeol, an iGDGT containing four cyclopentane rings and one cyclohexyl ring (43). The distribution of these moieties in natural systems is related to growth temperature and other environmental factors (44–48) and forms the basis of the TEX<sub>86</sub> paleo sea surface temperature proxy (41). At low pH and high temperatures, Archaea synthesize more highly-ringed moieties as an adaptation to maintain membrane rigidity and reduce permeability. In hydrothermal systems, the ring distributions of thermoacidophilic archaea record the interactions between temperature, pH, energy availability, and other factors that influence growth rate (48–50).

To better understand the signals recorded by archaeal lipid  $\delta^2\text{H}$  composition in natural systems, it is necessary to determine the extent to which environmental conditions influence  $^{2}\epsilon_{L/W}$  values. In this study, we determined the H-isotope fractionation between iGDGT-derived biphytanes and growth water ( $^{2}\epsilon_{L/W}$ ) for the thermoacidophilic and heterotrophic archaeon, *Sulfolobus acidocaldarius* (DSM 639). *S. acidocaldarius* evolved to grow optimally under multiple extreme conditions, namely low pH, high temperatures, and low oxygen partial pressure (51, 52). For this work, *S. acidocaldarius* was selected as a model organism because it thrives in extreme environments devoid of traditional eukaryotic lipid proxies (e.g., plant waxes) and because it can grow under a wide range of physicochemical conditions, with rapid doubling times and high biomass yields (53).

Here we cultivated *S. acidocaldarius* over a range of physicochemical conditions that included shifts in temperature, pH, shaking rate, electron acceptor, or electron donor flux. Changes in these environmental conditions are known to impact the growth rate and degree of iGDGT cyclization (47–49, 54, 55) but their impact on lipid/water fractionation is unexplored. Understanding how these environmental factors influence lipid/water fractionation is critical for interpreting archaeal lipid  $\delta^2\text{H}$  signatures in natural systems and refining their use as robust proxies for reconstructing past hydroclimate conditions.

## MATERIALS AND METHODS

### Culture strains and growth

Axenic cultures of *S. acidocaldarius* (DSM 639) were grown aerobically under different environmental conditions (Table 1). Culture media was prepared following the Brock recipe (56) with 5.9 mmol L<sup>-1</sup> (0.2% wt/vol) sucrose as the organic substrate. The electron donor flux experiments were also supplemented with 4.0 mmol L<sup>-1</sup> (0.1% wt/vol) NZ-amine in addition to sucrose.

Growth was monitored photometrically at regular intervals throughout each experiment by measuring the optical density (i.e., absorbance at 1 cm path length) of a culture aliquot at 600 nm (OD<sub>600</sub>) on a spectrophotometer. All experiments were inoculated to an initial OD<sub>600</sub> between 0.004 and 0.008, using cells derived from an active pre-culture (grown on the same medium) in the mid-exponential phase. Specific

TABLE 1 Summary of culture conditions and descriptive growth statistics for *S. acidocaldarius* grown over varying environmental conditions<sup>a</sup>

Experiment	Treatment	N	Culture conditions					Growth rate (hour <sup>-1</sup> )		Doubling time (hours)		Max OD <sub>600</sub>	
			T °C	pH	RPM <sup>b</sup>	O <sub>2</sub> %	δ <sup>2</sup> H <sub>W</sub> (‰)	Mean	sd	Mean	sd	Mean	sd
Temp (°C)	65	5	65	3	200	Air	-47.6	0.09	0.02	8.03	1.53	1.37	0.12
	70	5	70	3	200	Air	-55.0	0.10	0.01	7.07	0.65	1.96	0.14
	75	5	75	3	200	Air	-54.2	0.16	0.02	4.38	0.60	1.61	0.23
	80	5	80	3	200	Air	-52.7	0.19	0.01	3.73	0.19	1.65	0.21
pH	2	5	70	2	200	Air	-59.8	0.12	0.01	5.75	0.43	0.71	0.04
	3	5	70	3	200	Air	-55.0	0.10	0.01	7.07	0.65	1.96	0.14
	4	5	70	4	200	Air	-60.9	0.10	0.01	6.63	0.41	0.49	0.03
Aeration rate (RPM)	50	5	70	3	50	Air	-47.6	0.02	0.00	32.75	1.50	0.22	0.01
	125	5	70	3	125	Air	-46.3	0.08	0.00	8.82	0.51	0.73	0.01
	300	5	70	3	300	Air	-46.9	0.07	0.00	9.26	0.25	0.63	0.02
O <sub>2</sub> mixing ratio (%)	0.2%	3	70	3	200	0.2	-46.9	0.02	0.00	33.05	8.64	0.08	0.00
	0.5%	3	70	3	200	0.5	-55.6	0.05	0.02	14.17	4.54	0.10	0.00
	2%	3	70	3	200	2.0	-51.3	0.09	0.01	7.42	0.63	0.24	0.02
	20%	3	70	3	200	20	-51.0	0.34	0.21	2.58	1.36	0.32	0.04
e-donor flux (T <sub>D</sub> , hours)	7	6	70	2.25	200	20	-59.7	0.14	0.00	7.00	0.09	0.84	0.10
	21	9	70	2.25	200	20	-59.5	0.05	0.00	21.00	0.45	0.88	0.03
	44	6	70	2.25	200	20	-50.1	0.02	0.00	44.30	5.68	1.12	0.04

<sup>a</sup>δ<sup>2</sup>H<sub>W</sub> is the H-isotope composition of media water at the time of lipid sampling. Growth data for batch and fed-batch environmental condition experiments were initially reported by Cobban et al. (47), and growth data for the electron donor flux chemostat experiment were initially reported by Zhou et al. (48).

<sup>b</sup>For batch experiments, RPM is shaking rate; for bioreactor and chemostat experiments, RPM is impellor speed.

growth rates (division day<sup>-1</sup>; μ) were calculated using OD<sub>600</sub> measurements during the early to mid-exponential phase after Cobban et al. (47). Doubling time (T<sub>D</sub>) was calculated as

$$T_D (\text{hours}) = \ln(2)/\mu. \quad (1)$$

## Experimental conditions

We examined how temperature, pH, shaking rate, O<sub>2</sub> availability, and electron donor (sucrose) flux influence H-isotope fractionation in *S. acidocaldarius* through a series of batch, fed-batch, and chemostat experiments.

### Batch experiments

Three sub-experiments were performed in which one environmental condition (temperature, pH, or shaking rate) was systematically varied while holding the other two conditions constant (previously described in Cobban et al. [47]). The reference conditions were 70°C, pH 3, and 200 RPM shaking rate. Shaking rate is considered a proxy for aeration rate, where faster speeds increase oxygen availability in the media, though it also increases physical agitation.

Batch experiments were performed in temperature-controlled, shaking incubators (Innova-42, Eppendorf) in 250 mL Erlenmeyer flasks containing 125 mL media covered with loose plastic caps to reduce evaporation. Evaporation was further reduced by maintaining a 2 L tray of water in the incubator to humidify the atmosphere. All experiments were performed in quintuplicate. Biomass samples were collected in mid-exponential phase by centrifuging (3,214 × g; Eppendorf 5810 R, S-4-104 rotor) 50 mL of culture for 15 minutes at 4°C, the resulting cell pellets were stored at -80°C until lipid extraction.

### Fed-batch bioreactor experiments

To more precisely determine the impact of oxygen availability, we performed gas-fed batch experiments in bioreactors (previously described in Cobban et al. [47]). Briefly, *S.*

*acidocaldarius* was grown in 300 mL of medium in 1 L glass vessels. To modulate the availability (as flux) of the terminal electron acceptor O<sub>2</sub> was introduced to bioreactors at four different partial pressures: 0.2%, 0.5%, 2.0%, or 20% (balance N<sub>2</sub>). The O<sub>2</sub> dry mixing ratios 0.2%, 0.5%, and 2% were generated by mixing pure N<sub>2</sub> with 2% O<sub>2</sub> at 9:1, 3:1, and 0:1 ratios, respectively, which were controlled via my-Control PID controllers (Applikon, Delft, Netherlands). The 20% experiment used a separate gas feedstock of Ultra ZeroGrade Air (AirGas). Culture conditions were maintained at 70°C, pH 3, stirred at 200 RPM (Rushton-type impeller), and at a total gas flux of 200 mL min<sup>-1</sup>. Each experiment was performed in triplicate via three bioreactors operated in parallel. Biomass samples were collected by removing culture directly from the vessel, centrifuged at 4°C, to pellet biomass, and then stored at -80°C until lipid extraction.

### Chemostat experiments

To determine the impact of electron donor flux, we performed chemostat experiments in which the dilution rate of the growth vessel was set to yield cell doubling times (T<sub>D</sub>) of 7.0, 21.3, and 40.0 hours (previously described in Zhou et al. [48]). Briefly, *S. acidocaldarius* was grown in 300 mL of medium maintained at 70°C, pH 2.25, stirred at 200 RPM (Rushton-type impeller), and aerated with a constant flux of 200 mL min<sup>-1</sup> Zero Air (ultra-high purity, UHP, AirGas/AirLiquide, Inc.). Three chemostats were operated in parallel under continuous culture conditions. When the steady state was achieved (assessed via regular OD<sub>600</sub> measurements), biomass samples were harvested by continually collecting the outflow of each bioreactor into a chilled vessel (0°C to 4°C) for between 1 and 4 days, followed by centrifugation at 4°C and storage at -80°C prior to lipid processing. Multiple extracts representing 2 to 3 sampling events at identical growth rates were combined before lipid extraction.

### Lipid extraction and derivatization

Core lipid fractions (iGDGTs) were extracted from lyophilized cell pellets via acidic hydrolysis-methanolysis (45, 48). iGDGTs were chemically derivatized to biphytanes to permit the determination of the δ<sup>2</sup>H value of component biphytanes (10, 14). In brief, ether bonds were cleaved via digestion in 57% hydroiodic acid (HI) at 125°C for 4 hours. The resulting alkyl iodides were hydrogenated (e.g., reduced to biphytanes, BPs) in H<sub>2</sub>/PtO<sub>2</sub>. An isotope dilution occurs when H is added during hydrogenation, which is corrected during data processing and reduction (see “δ<sup>2</sup>H analysis of media waters, substrates, and biphytane lipids,” below).

### Lipid identities and distributions

Isoprenoid BP chains were analyzed via gas chromatography–mass spectrometry (Thermo ISQ LT with TRACE 1310) for compound identification and via GC-flame ionization detector (GC-FID; Thermo TRACE 1310) for compound quantification at the University of Colorado at Boulder Earth Systems Stable Isotope Lab (CUBES-SIL, Boulder, CO) (Fig. 1). Biphytane yields and recovery were calculated using GC peak areas and co-injected n-alkane mixture as a quantification standard.

To describe the average amount of cyclopentyl rings in each BP distribution, we calculated a BP-Ring Index based on the relative abundance of each BP moiety (equation 2). This metric is similar to the iGDGT-based Ring Index (equation 3), which describes the average amount of cyclopentyl rings in a distribution based on the relative abundance of each iGDGT moiety (48, 57).

$$RI_{BP} = \frac{(BP - 1) + (2 \cdot BP - 2) + (3 \cdot BP - 3)}{\sum_o^3 BP} \quad (2)$$

$$RI_{iGDGT} = \frac{(iGDGT - 1) + (2 \cdot iGDGT - 2) + (3 \cdot iGDGT - 3) + \dots + (8 \cdot iGDGT - 8)}{\sum_o^8 iGDGT} \quad (3)$$

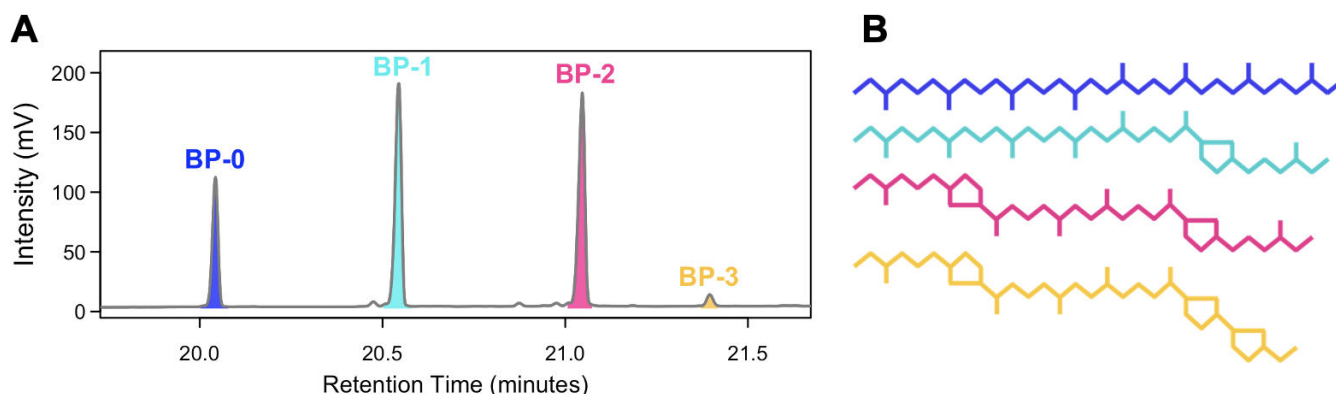


**FIG 1** (A) Representative chromatogram of intensity vs retention time for four iGDGT-derived BP moieties identified in *S. acidocaldarius* biomass that are named for the number of cyclopentane rings they contain. Although a BP-3 peak was detected, in many cases it is present in too low quantities to perform isotopic measurements. (B) Identity and structure of BP-0 to BP-3.

## $\delta^2\text{H}$ analysis of media waters, substrates, and biphytane lipids

### Media waters

Water samples for hydrogen isotope ( $\delta^2\text{H}$ ) analysis were collected concurrently with harvesting biomass for lipid analyses. Aliquots of filter-sterilized growth medium water was measured for  $\delta^2\text{H}$  at the Stable Isotope Laboratory at Dartmouth College via a dual inlet isotope ratio mass spectrometer (IRMS; Thermo Delta Plus 304 XL) coupled to an H-Device (pyrolyzed to  $\text{H}_2$  gas) for water reduction by chromium powder at  $850^\circ\text{C}$ . The  $\delta^2\text{H}_{\text{Water}}$  values were corrected using three laboratory standards spanning  $-161\text{‰}$  to  $-7\text{‰}$  vs Vienna standard mean ocean water (VSMOW), which were run every 8–10 samples. Analytical precision was  $<0.5\text{‰}$ .

### Substrates

The  $\delta^2\text{H}$  composition of non-exchangeable C-bound H from substrates used in growth media was analyzed in triplicate as trifluoroacetate derivatives via a Thermo Delta Plus XP coupled to a thermal conversion elemental analyzer (TC-EA) (58). The  $\delta^2\text{H}$  composition of sucrose was  $-93.0\text{‰} \pm 1.2\text{‰}$ .

### Biphytanes

For all experiments, we report  $^2\epsilon_{\text{LW}}$  values for BP hydrocarbons derived via ether cleavage from acid-extractable iGDGTs. The  $\delta^2\text{H}$  composition of individual BPs was determined by gas chromatography pyrolysis isotope ratio mass spectrometry (GC-P-IRMS) on a GC IsoLink II IRMS System (Thermo Scientific) at the University of Colorado at Boulder Earth Systems Stable Isotope Lab (CUBES-SIL, Boulder, CO). The system comprised a Trace 1310 GC fitted with a programmable temperature vaporization injector and either a 30 m ZB5HT column (i.d. = 0.25 mm, 0.25  $\mu\text{m}$ , Phenomenex, Torrance, CA, USA) or a 60 m DB1 column (i.d. = 0.25 mm, 0.25  $\mu\text{m}$ , Agilent, Santa Clara, CA, USA), ConFlo IV interface, and 253 Plus mass spectrometer (Thermo Scientific).

### Data reduction and notation

The  $\delta^2\text{H}$  values of individual biphytanes ( $\delta^2\text{H}_{\text{BP}}$ ) were measured relative to  $\text{H}_2$  reference gas ( $\delta^2\text{H}_{\text{raw}}$ ) and calibrated to the international references scale (VSMOW) using a standard n-alkane mixture (A7, containing C15 through C30 n-alkanes spanning  $-9\text{‰}$  to  $-263\text{‰}$  vs VSMOW; A. Schimmelmann, Indiana University). The A7 standard was combined with a  $\text{C}_{36}$  n-alkane ( $\text{nC}_{36}$ ,  $-259.2\text{‰}$  vs VSMOW; A. Schimmelmann, Indiana University) and measured throughout each analytical run at regular intervals and at different concentrations. The BP hydrogen isotope calibration was performed as in

Leavitt et al. (14), using the R packages *isoreader* (v 1.3.0) and *isoprocessor* (v 0.6.11) available at [github.com/isoverse](https://github.com/isoverse) (59). In brief,  $\delta^2\text{H}_{\text{raw}}$  values were corrected for offset, scale compression, and peak-size effects using an inverted multivariate linear regression which was applied to all standards and samples to determine  $\delta^2\text{H}_{\text{cal}}$  values. Further details of calibration and data reduction are available in Leavitt et al. (14). The total analytical uncertainty of the corrected  $\delta^2\text{H}_{\text{BP}}$  values was calculated using standard error propagation of the peak-size adjusted error estimates and hydrogenation correction assuming all errors to be uncorrelated. The hydrogenation correction ranged from 10.3‰ to 12.7‰ and increased analytical uncertainty by up to 1.9‰.

All  $^2\text{H}/^1\text{H}$  ratios are reported in delta notation ( $\delta^2\text{H}$ ) in permil (‰) units relative to the international seawater standard on the VSMOW-SLAP (Vienna Standard Mean Ocean Water, Standard Light Antarctic Precipitation) scale.

$$\delta^2\text{H} (\text{‰}) = \left( \frac{^2\text{H}/^1\text{H}_{\text{Sample}}}{^2\text{H}/^1\text{H}_{\text{Standard}}} - 1 \right) \quad (4)$$

All fractionation factors are reported in epsilon notation ( $^2\epsilon$ ) in permil (‰) units. The hydrogen isotope fractionation between growth water and BP lipids ( $^2\epsilon_{\text{L/W}}$ ) is calculated as:

$$^2\alpha_{\text{L/W}} = \frac{^2\text{H}/^1\text{H}_{\text{BP}}}{^2\text{H}/^1\text{H}_{\text{Water}}} \quad (5a)$$

$$^2\epsilon_{\text{L/W}} (\text{‰}) = (^2\alpha_{\text{L/W}} - 1) \quad (5b)$$

Corrected  $\delta^2\text{H}_{\text{BP}}$  values and resulting  $^2\epsilon_{\text{L/W}}$  fractionation factors from biological replicates ( $n \geq 1$ ) and analytical replicates ( $n \geq 3$ ) were averaged for each experimental condition. All averages are weighted means of individual measurements ( $1/\sigma^2$  weights) to account for the amplitude-dependent range in uncertainties. The reported error estimate of each average is the larger of the standard deviation of all replicates or the propagated uncertainty from individual measurements. Abundance weighted averages for  $\delta^2\text{H}_{\text{BP}}$  and  $^2\epsilon_{\text{L/W}}$  values include all BPs with relative abundance  $>5\%$ .

The ring difference ( $\Delta\epsilon/\text{ring}$ ), or changes in  $^2\epsilon_{\text{L/W}}$  with an increasing number of ring structures is calculated for all pairwise combinations of  $^2\epsilon_{\text{L/W}}$  values after Leavitt et al. (14), where X and Y refer to the ring number of BP moieties and  $X > Y$ :

$$\frac{\Delta\epsilon}{\text{ring}} (\text{‰}) = \frac{^2\epsilon_{\text{L/W}}(\text{X}) - ^2\epsilon_{\text{L/W}}(\text{Y})}{(\text{X} - \text{Y})} \quad (6)$$

The raw data and code for all data manipulations and statistical analyses are archived (60) and available on GitHub ([https://github.com/carolynnharris/Saci\\_Enviro\\_d2H](https://github.com/carolynnharris/Saci_Enviro_d2H)).

## RESULTS

We examined how temperature, pH, shaking rate,  $\text{O}_2$  availability, and electron donor (sucrose) flux influence H-isotope fractionation in *S. acidocaldarius* through a series of batch, fed-batch, and chemostat experiments. Details of the growth responses and lipid iGDGT profile responses to these conditions can be found in Cobban et al. (47), and Zhou et al. (48). In brief, each environmental condition independently influences growth rate, the relative abundance of many subsets of iGDGT core lipids, and the RI-GDGT (47, 48) (Table 1; Fig. 2A through E; Fig. S1).

Here, we show that each environmental condition also influences the relative abundance of BP lipids and the RI-BP (Table 2; Fig. 2F through O). Among all samples, the relative abundance of biphytanes averaged 13%, 30%, 49%, and 7% for BP-0, -1, -2, and -3, respectively; BP-3 was the least abundant and was not measurable in some samples. RI-BP ranged from 1.01 to 2.04 and, as expected, was positively correlated with RI-GDGT

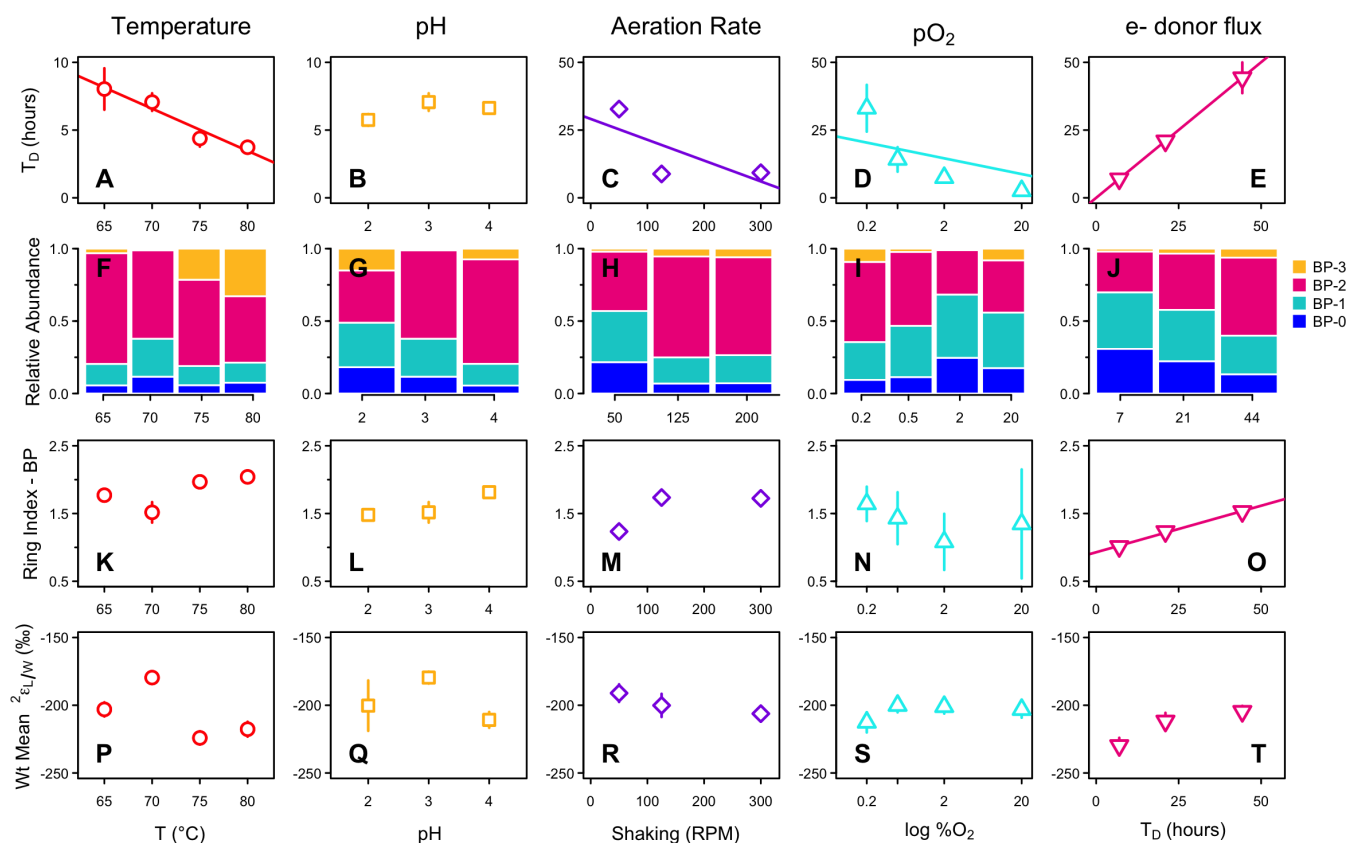


**FIG 2** Results for *S. acidocaldarius* grown under varying environmental conditions. Top row (A–E): doubling time in response to each environmental condition. Second row (F–J): relative abundance of BP lipids derived from iGDGTs. BP-3 was the least abundant and was below the detection limit in some samples. Bars represent the mean across replicates for each treatment level. Third row (K–O): ring index (RI-BP) of biphytane lipids derived from iGDGTs. Bottom row (P–T): the abundance-weighted mean H-isotope fractionation ( $^2\epsilon_{L/W}$ ) between growth water and biphytanes. For all rows, points represent the mean and propagated error across biological and technical replicates for each treatment level. In many cases, error bars are smaller than symbols. Only statistically significant regressions are shown ( $P < 0.05$ ).

( $R^2 = 0.52$ ,  $P = 0.001$ , Fig. S2). Among all samples, the abundance-weighted mean  $\delta^2H_{BP}$  values range from  $-276\text{‰}$  to  $-225\text{‰}$  and were consistently depleted in  $^2H$  relative to growth water, corresponding to  $^2\epsilon_{L/W}$  values from  $-230\text{‰}$  to  $-180\text{‰}$  (Table 3; Fig. 2P through T).

Despite significant effects on growth rate and lipid cyclization, individual environmental parameters had minimal impact on  $^2\epsilon_{L/W}$  values, which spanned a range of 44‰, 31‰, 15‰, 21‰, and 25‰ in the temperature, pH, shaking rate,  $O_2$  availability, and electron donor flux experiments, respectively. We observed a weak linear relationship between environmental conditions and  $^2\epsilon_{L/W}$  only in the electron donor flux experiment, where larger doubling times are associated with slightly less negative  $^2\epsilon_{L/W}$  values (smaller offset from water) ( $R^2 = 0.89$ ,  $P = 0.22$ , slope =  $0.72\text{‰} \pm 0.25\text{‰}/\text{hour}$ ) (Fig. 2T).

In the batch and fed-batch experiments,  $^2\epsilon_{L/W}$  values for individual BPs showed no consistent pattern with an increasing number of cyclic moieties, and the ring difference ( $\Delta\epsilon/\text{ring}$ ) varied widely in direction and magnitude among all treatments ( $-39\text{‰}$  to  $+24\text{‰}$ ) (Table 3; Fig. 3A through D; Fig. S3A through D). The variability in mean  $\Delta\epsilon/\text{ring}$  was smaller, though still not of uniform direction, with values ranging from  $-5.4\text{‰}$  to  $+10.2\text{‰}$  (Table 3; Fig. S4A through D). In contrast,  $^2\epsilon_{L/W}$  values in the chemostat experiment generally increased with the number of cyclic moieties, showing offsets of 3.7‰, 4.1‰, and 10.1‰ for BP-1, BP-2, and BP-3 relative to BP-0 (Table 3; Fig. 3E; Fig. S3E). Similarly, the mean ring difference ( $\Delta\epsilon/\text{ring}$ ) was uniformly positive and showed

**TABLE 2** Relative abundance of individual biphytanyl (BP) lipids and Ring Index for iGDGT-derived BPs for *S. acidocaldarius* grown under varying environmental conditions<sup>a</sup>

Experiment	Treatment	N	BP-0		BP-1		BP-2		BP-3		Ring Index	
			Rel Abund	sd	mean	sd						
Temp (°C)	65	1	0.06	0.00	0.15	0.01	0.76	0.00	0.03	0.00	1.77	0.01
	70	1	0.12	0.04	0.26	0.03	0.61	0.07	0.01	0.00	1.52	0.15
	75	1	0.06	0.01	0.13	0.01	0.60	0.02	0.21	0.02	1.97	0.07
	80	1	0.07	0.01	0.14	0.00	0.46	0.01	0.33	0.01	2.04	0.02
pH	2	1	0.18	0.00	0.31	0.00	0.36	0.00	0.15	0.00	1.48	0.00
	3	1	0.12	0.04	0.26	0.03	0.61	0.07	0.01	0.00	1.52	0.15
	4	1	0.05	0.00	0.15	0.01	0.72	0.01	0.07	0.00	1.81	0.02
Aeration rate (RPM)	50	1	0.22	0.01	0.35	0.02	0.41	0.01	0.02	0.00	1.23	0.02
	125	1	0.07	0.00	0.18	0.01	0.70	0.01	0.05	0.00	1.74	0.03
	300	1	0.07	0.00	0.19	0.01	0.68	0.01	0.06	0.00	1.72	0.01
O <sub>2</sub> mixing ratio (%)	0.2%	2	0.09	0.02	0.26	0.05	0.55	0.06	0.09	0.01	1.64	0.25
	0.5%	1	0.11	0.02	0.35	0.07	0.51	0.09	0.02	0.01	1.43	0.38
	2%	3	0.25	0.01	0.44	0.00	0.31	0.02	0.01	0.00	1.08	0.41
	20%	3	0.18	0.02	0.38	0.05	0.36	0.05	0.08	0.12	1.35	0.80
e-donor flux (T <sub>D</sub> , hours)	7	1	0.31	0.00	0.39	0.01	0.28	0.00	0.02	0.00	1.01	0.01
	21	1	0.22	0.00	0.35	0.00	0.39	0.00	0.03	0.00	1.23	0.02
	44	1	0.13	0.00	0.27	0.00	0.54	0.01	0.06	0.00	1.53	0.02

<sup>a</sup>The Ring Index describes the relative abundance of BP moieties in a sample. Mean and sd include biological replication ( $N \geq 1$ ) and technical replication (e.g., multiple injections,  $n \geq 3$ ).

little variation among doubling times, ranging from 4.9‰ to 9.2‰ (Table 3; Fig. S4E). On average in continuous culture, each additional ring contributes a  $7.4‰ \pm 2.2‰$  increase to biphytane  $^{2}\epsilon_{L/W}$ .

Correlation matrices show the linear relationship between each environmental condition, growth parameters (doubling time and maximum OD<sub>600</sub>), mean lipid cyclization indices (RI-BP and RI-GDGT),  $\Delta\epsilon/\text{ring}$ , and abundance weighted  $^{2}\epsilon_{L/W}$  values for each environmental condition experiment (Fig. 4). These plots further demonstrate that the minimal variation in  $^{2}\epsilon_{L/W}$  observed within each experiment is not related to variation in the experimentally manipulated environmental conditions or any other measured parameter.

To explore the possibility that lipid/water fractionation is related to optimal growth, we relate abundance weighted mean  $^{2}\epsilon_{L/W}$  values to doubling time for each environmental condition (Fig. 5A through E). To allow for comparisons among all environmental conditions, we also relate  $^{2}\epsilon_{L/W}$  to doubling time for all experiments combined. In this pooled data set, abundance weighted mean  $^{2}\epsilon_{L/W}$  values range from  $-230‰$  to  $-180‰$  (mean =  $-204‰ \pm 12‰$ , based on 22 biological replicates; Table 3) and showed no correlation to doubling time (Fig. 5,  $R^2 = 0.0$ ,  $P = 0.97$ ), indicating a decoupling between lipid/water fractionation and growth rate.

## DISCUSSION

### Effect of environmental conditions on archaeal lipid $^{2}\epsilon_{L/W}$ values

The primary goal of this work was to investigate the impact of environmental conditions on lipid/water fractionation in archaeal lipids, which relates to their potential as archives of hydroclimate across space and time. The conditions tested in this study were chosen to encompass the natural conditions of thermoacidophilic archaea, which are globally distributed in hot, acidic features including fumaroles (steam-saturated discharges) as geysers and pools in the terrestrial environment, and hydrothermal vents in the marine environment (61). Both realms experience steep and rapidly changing gradients in temperature, pH, oxygen, and dissolved solute concentrations, which can

**TABLE 3** Isotope results for individual BP lipids derived from iGDGTs for *S. acidocaldarius* grown under varying environmental conditions, including H-isotope composition ( $\delta^2\text{H}_{\text{BP}}$ , ‰), lipid/water fractionation ( $^2\epsilon_{\text{L/W}}$ , ‰), and ring difference ( $\Delta\epsilon/\text{ring}$ , ‰)<sup>a</sup>

Exp.	Treatment	BP-0			BP-1			BP-2			BP-3 <sup>b</sup>			Abundance weighted mean											
		$\delta^2\text{H}$ (‰)	sd	$^2\epsilon_{\text{L/W}}$ (‰)	$\delta^2\text{H}$ (‰)	sd	$^2\epsilon_{\text{L/W}}$ (‰)	$\delta^2\text{H}$ (‰)	sd	$^2\epsilon_{\text{L/W}}$ (‰)	$\delta^2\text{H}$ (‰)	sd	$^2\epsilon_{\text{L/W}}$ (‰)	$\delta^2\text{H}$ (‰)	sd	$^2\epsilon_{\text{L/W}}$ (‰)	$\Delta\epsilon/\text{ring}$	sd	$\Delta\epsilon/\text{ring}$						
Temp (°C)	65	-234	18	-195	19	-232	5	-193	5	2	19	-243	3	-205	3	-9	n.d.	n.d.	-241	6	-203	5	-5	0	
	70	-221	8	-175	9	-225	5	-180	5	-5	10	-225	3	-180	3	-2	n.d.	n.d.	-225	5	-180	4	-3	0	
	75	-262	4	-220	5	-256	4	-214	5	6	7	-268	5	-226	6	-8	4	-268	4	-227	4	-3	3	2	
	80	-253	13	-211	13	-248	6	-206	7	5	15	-262	5	-221	5	-10	6	-260	3	-219	3	-2	3	3	
pH	2	-258	25	-211	27	-252	19	-205	20	6	34	-248	11	-200	11	5	14	-228	22	-179	24	15	11	-248	22
	3	-221	8	-175	9	-225	5	-180	5	-5	10	-225	3	-180	3	-2	4	n.d.	n.d.	n.d.	n.d.	n.d.	n.d.	-225	4
	4	-249	9	-201	10	-251	6	-202	6	-1	12	-261	5	-214	6	-9	5	-257	6	-209	7	-1	4	-259	5
RPM	50	-230	3	-192	3	-227	5	-189	5	3	6	-232	4	-193	4	-3	4	-222	34	-183	36	5	14	-230	6
	125	-235	12	-198	12	-231	7	-194	7	4	15	-239	7	-202	7	-5	6	-239	21	-202	22	-2	9	-237	9
	300	-238	6	-201	7	-240	5	-202	5	-2	8	-244	2	-207	2	-4	3	-254	13	-217	13	-8	5	-243	4
O <sub>2</sub> mixing ratio (%)	0.2%	-244	2	-208	8	-275	7	-239	3	-31	5	-231	13	-193	17	20	3	-231	9	-194	15	12	1	-248	9
	0.5%	-255	5	-211	5	-237	4	-192	5	11	8	-239	5	-194	6	5	4	n.d.	n.d.	n.d.	n.d.	n.d.	n.d.	-244	4
	2%	-243	5	-202	6	-242	2	-201	4	1	0	-242	4	-200	5	1	0	n.d.	n.d.	n.d.	n.d.	n.d.	n.d.	-242	5
	20%	-243	1	-202	1	-243	4	-202	5	0	2	-246	5	-205	5	-2	1	n.d.	n.d.	n.d.	n.d.	n.d.	n.d.	-244	5
e-donor flux	7	-280	7	-234	7	-276	4	-230	4	4	8	-272	6	-226	5	4	4	-253	17	-205	19	14	8	-276	6
	21	-261	6	-214	6	-261	5	-214	6	0	8	-257	5	-210	5	3	4	-237	18	-189	20	14	8	-259	5
	44	-253	4	-214	5	-246	6	-207	6	7	7	-242	3	-202	3	5	4	-239	5	-199	5	4	2	-244	4

<sup>a</sup>Mean and sd include biological replication (N ≥ 1) and technical replication (e.g., multiple injections, n ≥ 3). Abundance-weighted means across all BPs are shown for  $\delta^2\text{H}_{\text{BP}}$ ,  $^2\epsilon_{\text{L/W}}$ , and  $\Delta\epsilon/\text{ring}$  values with propagated error.

<sup>b</sup>For BP-3, no data (n.d.) indicates this moiety was present in too low concentrations to reliably measure the H-isotope composition.

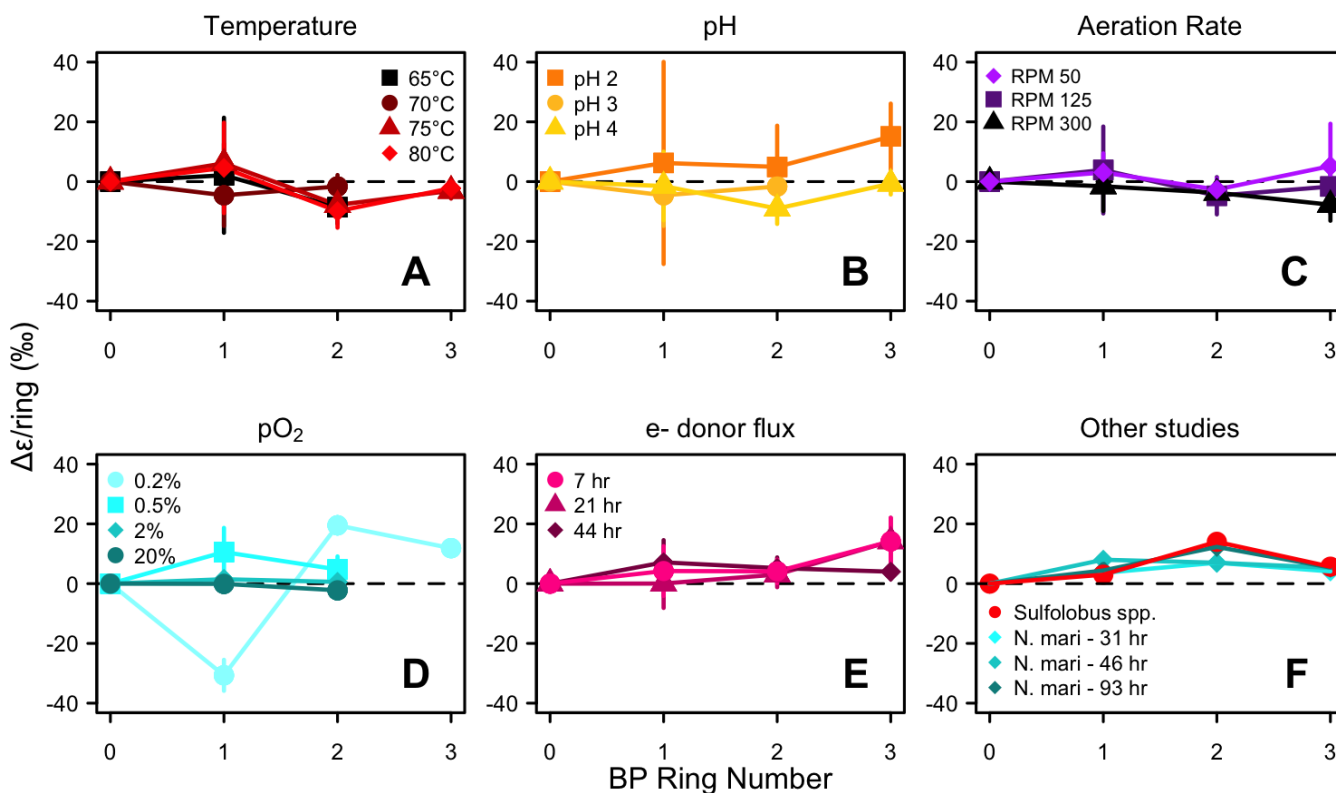


**FIG 3** (A–E) Ring difference ( $\Delta\epsilon/\text{ring}$ , ‰) for individual biphytanes in each environmental condition experiment. BP-0 has a  $\Delta\epsilon/\text{ring}$  of 0 by definition and is shown for reference. BP-3 was not recovered from every treatment. Note the axes are scaled differently for each plot. Points represent the mean of biological and technical replicates for each treatment level. (F) Ring difference for biphytanes examined in other studies. Blue diamonds are *N. maritimus* from Leavitt et al. (14); red squares are *Sulfolobus* sp. from Kaneko et al. (10). Kaneko et al. also recovered BP-4 from *Sulfolobus* spp. (data not shown); the  $\Delta\epsilon/\text{ring}$  for BP-4 is 11.7‰.

disturb ecological niches (62). As a result, Archaea have adapted to or evolved strategies to mitigate these challenges (61, 63).

In *S. acidocaldarius*, our experimental manipulations of temperature, pH, shaking rate, electron acceptor ( $O_2$ ) availability, and electron donor (sucrose) flux elicited a 20-fold change in growth rate and twofold change in mean biphytane cyclization (RI-BP), but  $^2\epsilon_{L/W}$  values were largely invariant ( $-204\text{‰} \pm 12\text{‰}$ ,  $n = 22$ ). This finding is consistent with previous studies that show archaeal lipids are consistently  $^2H$ -depleted relative to source water and display a narrow range of  $^2\epsilon_{L/W}$  values despite considerable variation in taxonomy, metabolic mode, and growth conditions (10–15) (Fig. 6).

In heterotrophic archaea, lipid-bound H can originate from water or the organic substrate used for growth, with intracellular hydride carriers, such as NADPH, mediating the incorporation of H from both sources into lipids (11, 33, 38). In heterotrophs, the NADPH incorporated into lipid products inherits some H from the available organic substrate(s). While there are several potential mechanisms by which each environmental stressor tested here could influence lipid/water fractionation in archaea, our data suggest these processes either do not occur or are insufficient to cause a measurable effect. Temperature, pH, oxygen levels, and nutrient availability are known to trigger physiological responses in archaea, including changes in growth rates, membrane lipid composition, and enzyme activity (47, 48, 52, 65). Enzyme kinetics, which is influenced by growth temperature and oxidative stress (66), could affect lipid/water fractionation if the enzyme catalyzing hydrogen transfer is associated with a significant isotope effect (33). High temperatures and low pH reduce water exchange across archaeal membranes to prevent osmotic stress (65), which could enrich the intracellular water in  $^2H$  and potentially reduce apparent lipid/water fractionation (67). Additionally, changes in electron donor availability can shift the pathway by which NADPH is reduced, which could

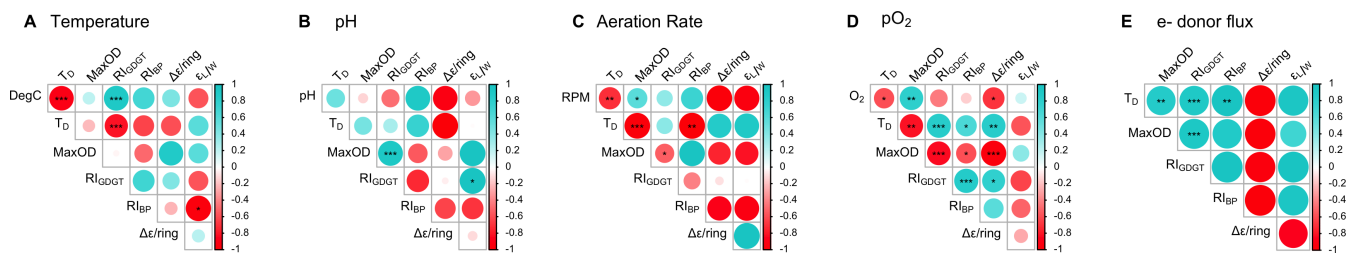


**FIG 4** Correlation matrices showing linear relationships among environmentally manipulated parameters, growth statistics (doubling time [ $T_D$ ] and maximum OD<sub>600</sub>), mean cyclization of lipids (RI-GDGT and RI-BP), ring difference, and abundance weighted mean  $^2\epsilon_{L/W}$  for (A) temperature, (B) pH, (C) aeration rate, (D) O<sub>2</sub> mixing ratio, and (E) electron donor flux. Notably, mean  $^2\epsilon_{L/W}$  values do not show a strong linear correlation to any other measured parameter, indicating that environmental conditions, growth statistics, and mean cyclization do not significantly influence the degree of lipid/water fractionation in *S. acidocaldarius*. Circle color and size indicate the strength and direction (blue = correlated, red = anticorrelated) of the relationship. Significance levels: \* $P < 0.05$ , \*\* $P < 0.001$ , \*\*\* $P < 0.0001$ . Circles without a star indicate the relationship is not statistically significant.

influence the  $\delta^2\text{H}$  composition of NADPH, which ultimately supplies protons to lipid products (68, 69). For example, methanogenic archaea switch between the reductive acetyl-CoA and  $F_{420}$ -dependent hydrogenase systems depending on whether electron donors ( $\text{H}_2$  or formate) are abundant or limiting (68). Despite these possible mechanisms, lipid/water fractionation in *S. acidocaldarius* remains largely invariant in each experiment, indicating that these processes either do not occur or are not significant enough to alter

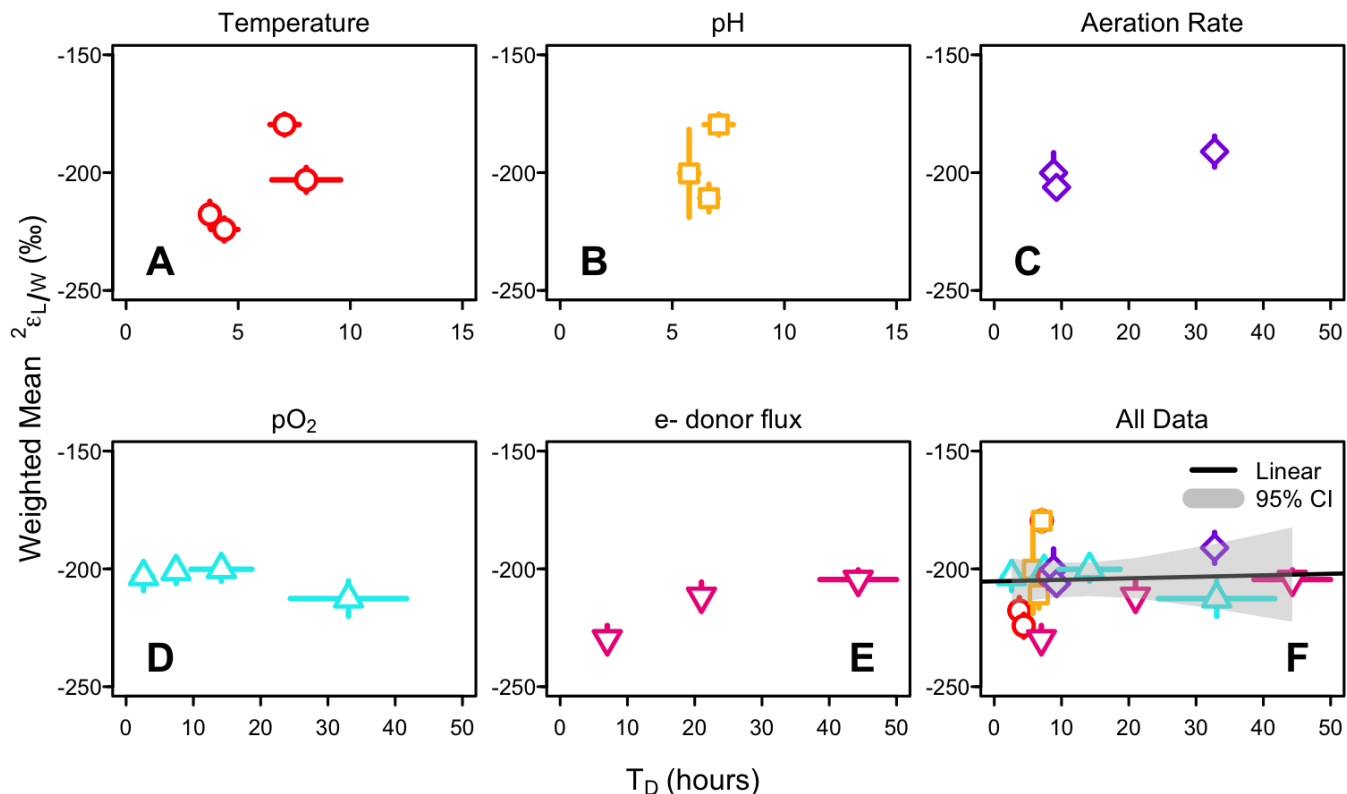


**FIG 5** The abundance-weighted H-isotope fractionation ( $^2\epsilon_{L/W}$ ) between growth water and BPs in response to doubling time (hours) in each environmental condition experiment (A–E) and pooled across all experiments (F). When data from all environmental control experiments are pooled, there is no relationship between doubling time (hours) and abundance weighted mean  $^2\epsilon_{L/W}$ . Points represent the mean of biological and technical replicates for each treatment level. Error bars represent propagated error associated with BP abundance measurements, BP- $\delta^2\text{H}$  measurements, and weighted mean  $^2\epsilon_{L/W}$  calculations; bars are smaller than the symbols in many cases.

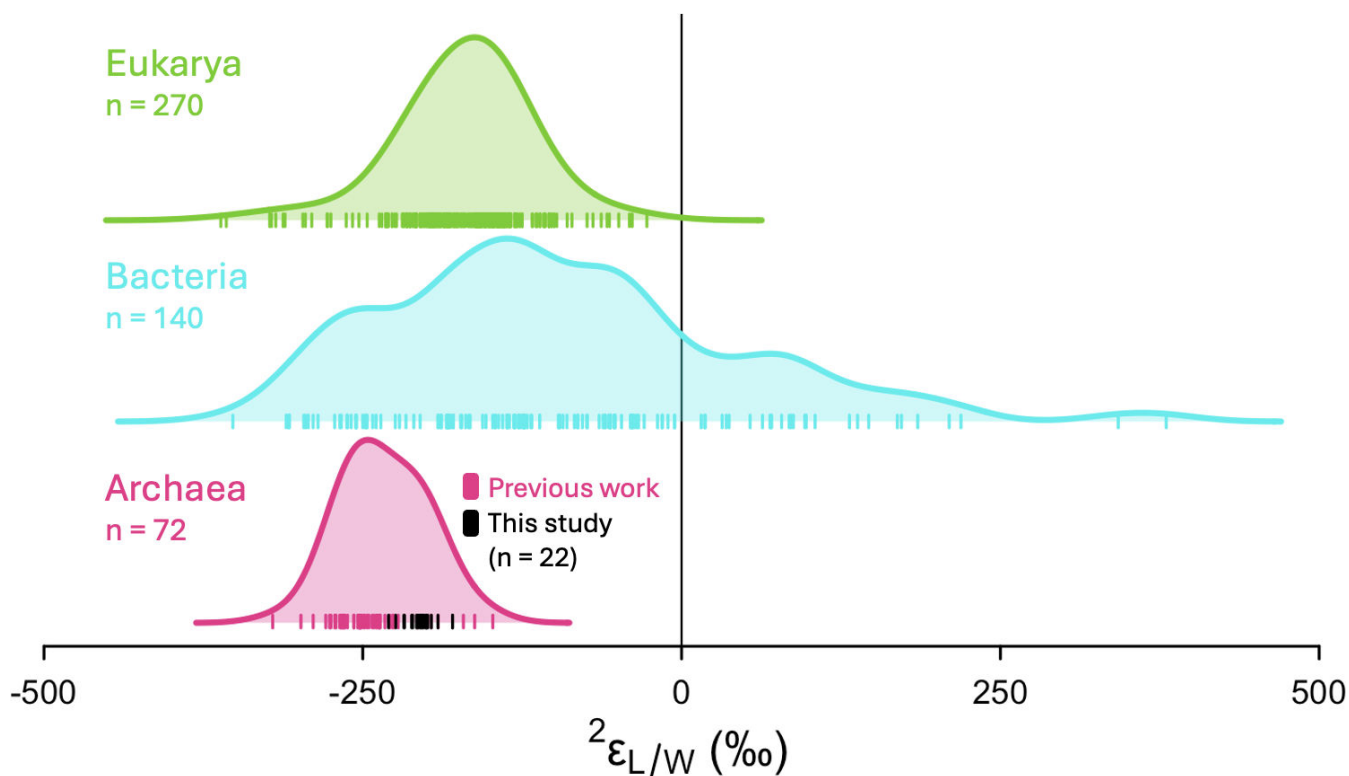


**FIG 6** Summary of lipid/water fractionation ( $^2\epsilon_{L/W}$ ) values measured in culture studies across three domains of life: eukaryotic phototrophs (green;  $n = 270$ ), bacteria (blue;  $n = 140$ ), and archaea (pink;  $n = 72$ ). Tick marks indicate individual  $^2\epsilon_{L/W}$  values; shaded curves indicate probability density functions. Archaea data include measurements of phytanes and biphytanes from *Sulfolobus* sp. (10), *M. barkeri* (13), *N. maritimus* (64), *Acidianus* sp. DS80, *A. fulgidus*, *Metallosphaera sedula* (15), and *S. acidocaldarius* (this study; black tick marks). Data for Eukarya and Bacteria are redrawn from Rhim et al. (15), Fig. 6. Eukarya data include measurements for acetogenic and isoprenoid lipids. Bacteria data include fatty acids synthesized by multiple metabolisms (e.g., aerobic and anaerobic heterotrophy, aerobic and anaerobic chemoautotrophy, and photoautotrophy).

fractionation under the tested conditions. An alternative hypothesis is that *S. acidocaldarius* maintains a constant internal metabolic balance, particularly in NADPH production and utilization, regardless of external conditions.

Physiological responses to stressors impact growth rate and examining  $^2\epsilon_{L/W}$  values in response to optimal vs suboptimal growth may provide a more coherent explanation for the non-linear patterns we observe across the environmental conditions tested. The  $^2\epsilon_{L/W}$  values for *S. acidocaldarius*, however, are not correlated to the growth rate in any single environmental condition experiment or when data for all conditions are pooled. This finding suggests that cells maintain stable internal metabolic processes resulting in a consistent H-balance over a range of growth rates and is consistent with the theory that a constant lipid/water fractionation is a feature of an imperturbable central energy metabolism (14, 15). *S. acidocaldarius*, like most archaea, employs energy-efficient metabolic strategies (70, 71), possibly as an adaptation to energy-limiting environments (63, 72). In tightly controlled metabolic pathways, the balance between the supply and use of NADPH-reducing power appears to remain constant, even under energy-stress conditions. Previous research suggests archaea may exist in a permanent state of NADPH deficiency such that all NADPH is immediately used for biosynthesis with little to no flux from NADPH back to NADH (14). This efficiency in NADPH use may explain why changing growth rates do not impact kinetic isotope effects associated with biosynthesis and hydride exchange. NADPH deficiency (deemed NADPH flux imbalance by Wijker et al. (38), is associated with energy limitation, and can provide a framework to relate patterns in  $^2\epsilon_{L/W}$  values to the fluxes of H through dehydrogenase and transhydrogenase enzymes. Indeed, NADPH flux imbalance may explain why all archaea (to date) and

autotrophic and obligately anaerobic bacteria display negative  ${}^2\epsilon_{L/W}$  values of similar magnitude (15, 33, 36, 38). This similarity is striking given that fatty acids and isoprenoid GDGTs are formed via different biosynthetic pathways and suggests that the ultimate control on  ${}^2\epsilon_{L/W}$  values may be related to free energy yields (15).

Both the  $O_2$  availability and sucrose flux experiments test the hypothesis that energy limitation—either terminal electron acceptor or donor—can alter  ${}^2\epsilon_{L/W}$  values in archaea. These experiments produced the largest range in doubling times (2 to 50 hours and 7 to 44 hours in the  $O_2$  availability and electron donor experiments, respectively); yet  ${}^2\epsilon_{L/W}$  values remained fairly consistent ( $-217\text{‰}$  to  $-196\text{‰}$  and  $-276\text{‰}$  to  $-244\text{‰}$ , respectively). *N. maritimus* is the only other archaeon in which the relationship between electron donor (ammonium) flux and lipid/water fractionation was examined; this archaeon similarly exhibited no significant correlation between a threefold change in doubling time and  ${}^2\epsilon_{L/W}$  values ( $R^2 = 0.22$ ,  $P = 0.07$ , slope =  $0.18\text{‰} \pm 0.09\text{‰/hour}$ ) (14). The authors speculate this strain maintains a consistent H-balance over a range of electron donor fluxes as an adaptation that allows cells to perform nitrification with energy-efficient  $CO_2$  fixation in oligotrophic environments (14). These findings suggest that archaea with diverse physiologies (e.g., heterotrophy vs chemoautotrophy, extremophily vs mesophily) maintain a constant lipid-to-water fractionation that is minimally affected by free energy availability and may reflect the fact that Archaea are adapted to chronic energy limitation (63, 72). This stability may reflect tightly regulated physiological processes, such as isoenzyme switching and modulation of enzyme activities, which help maintain metabolic homeostasis under both optimal and sub-optimal growth conditions (73). In contrast, in bacteria and some planktonic eukaryotes faster growth is associated with larger lipid/water fractionation (67, 74, 75), and  ${}^2\epsilon_{L/W}$  values for bacteria are influenced by electron donor flux (33, 36, 38).

The only other study in archaea to examine the relationship between environmental conditions and lipid/water fractionation cultured the halophilic heterotrophic archaeon, *H. marismortui* (which produces archaeol diethers), under varying temperatures and salinities when grown on complex rich medium (11). The resulting  ${}^2\epsilon_{\text{Archaeol/W}}$  values are relatively invariant (ranging from  $-126\text{‰}$  to  $-143\text{‰}$ ; more enriched than our observations for *S. acidocaldarius*) and are decoupled from growth rate (Fig. S5;  $R^2 = 0.07$ ,  $P = 0.7$ , slope =  $0.85\text{‰} \pm 1.84\text{‰/hour}$ ), providing more evidence that archaea maintain a stable internal H-balance across a range of growth conditions (11).

The impact of the growth phase on H-isotope dynamics has not been studied in depth. The batch and fed-batch experiment techniques used here for *S. acidocaldarius* and in the *H. marismortui* study integrate across growth stages, whereas the chemostat electron donor flux experiments for *S. acidocaldarius* and *N. maritimus* achieve constant growth rates. A recent study grew *A. fulgidus* in batch cultures and found that  ${}^2\epsilon_{L/W}$  values were more depleted (larger offset from water) during the exponential phase relative to the stationary phase (15). This pattern was consistent between heterotrophic and autotrophic experiments. The culture conditions in Rhim et al. resulted in a threefold difference in growth rates (similar change to the *N. maritimus* study, but a much smaller range than the 20-fold change we report for *S. acidocaldarius* here) and a 50‰ change in  ${}^2\epsilon_{L/W}$  values ( $-280\text{‰}$  to  $-230\text{‰}$ ). Rhim et al. conclude that both metabolic mode (heterotrophic vs autotrophic growth) and growth phase impact  ${}^2\epsilon_{L/W}$  values, though the total variance among all treatments was small and overlapped with ranges reported for other archaea (15).

### Effect of biphytane ring number on archaeal lipid ${}^2\epsilon_{L/W}$ values

Stoichiometric modeling predicts that BPs with more rings incorporate less of the highly-fractionated hydrogen donated through GGR reduction, a process where the enzyme geranyl-geranyl reductase (GGR) catalyzes the reduction of double bonds in isoprenoid chains, thereby affecting the isotopic composition of the resulting lipids (14). Interestingly, in our *S. acidocaldarius* work, this stepwise enrichment is only seen in the chemostat experiments, where each additional ring contributes  $7.4\text{‰} \pm 2.2\text{‰}$  to

biphytane  $^{2}\epsilon_{L/W}$  values. In the batch and fed-batch experiments, there is no consistent dependence of  $^{2}\epsilon_{L/W}$  values on the number of biphytane moieties. In particular, the  $\Delta\epsilon/\text{ring}$  trends differ between the shaking rate and  $\text{O}_2$  availability experiments, which likely reflects the fact that the shaking rate can also impart stress via physical agitation in addition to increasing oxygenation of microbial media (47).

iGDGT-derived BPs extracted from marine sediments also lack a clear stepwise enrichment with increasing ring moieties (10) but this likely occurs because sediments integrate lipids synthesized by different populations of archaea that are either growing on multiple substrates or in different water masses (10). It is less clear why the pure *S. acidocaldarius* batch and fed-batch cultures do not display a ring-specific pattern, though it perhaps relates to variations in biosynthetic fractionations accompanying changes in lipid biosynthesis across the growth phases (44). Considering all the available data, this enrichment pattern appears only minimally affected by differences in growth rate and metabolism, as the magnitude of per-ring increase in  $^{2}\epsilon_{L/W}$  value is similar for *Sulfolobus* sp. (10), *S. acidocaldarius* (chemostat experiment in this study), and *N. maritimus* (14), which collectively represent a fivefold range of growth rates and a variety of metabolisms and carbon substrates (*Sulfolobus* sp. = yeast extract +  $\text{O}_2$ ; *S. acidocaldarius* = sucrose +  $\text{O}_2$ ; *N. maritimus* = chemoautotroph on  $\text{NH}_4 + \text{O}_2$ ). The magnitude of this stepwise enrichment, however, is small and would likely have a minor impact (usually <10‰) on the abundance-weighted mean  $^{2}\epsilon_{L/W}$  value even in cases where the BP Ring Index was markedly different among samples.

### Archaeal lipid $^{2}\epsilon_{L/W}$ as a function of central metabolism

The *S. acidocaldarius*  $^{2}\epsilon_{L/W}$  values we report are broadly similar to results from previous experimental investigations of the *Sulfolobus* genus cultured heterotrophically. When grown at 75°C and pH 2 on yeast extract, a *Sulfolobus* strain displayed  $^{2}\epsilon_{L/W}$  values from -213‰ to -161‰ for BP-0 to -4 (abundance weighted mean = -180‰ (10) vs -204‰  $\pm$  12‰ for *S. acidocaldarius* here). In another study, *Sulfolobus solfataricus* grown at 76°C and pH 3.5 on glutamate displayed more enriched  $^{2}\epsilon_{L/W}$  values, averaging -134‰ when intact iGDGT-1 and -2 were analyzed (12). The difference in  $^{2}\epsilon_{L/W}$  values may in part be due to the structures analyzed. Lengger et al. analyzed intact iGDGTs including the glycerols which may enrich the  $\delta^2\text{H}_{\text{iGDGT}}$  composition, though the different substrates may also play a role (12). Glutamate, an amino acid, is a more complex substrate than simple sugars (such as sucrose) and primarily enters the *Sulfolobus* central metabolism through the TCA cycle (76). Simple sugars enter metabolism primarily through the Entner-Doudoroff pathway, which converts the sugar to intermediates that feed into the TCA cycle (76).

When *S. acidocaldarius* is grown heterotrophically on a simple sugar (glucose), the weighted mean  $\delta^2\text{H}$  composition of biphytane lipids is strongly correlated with  $\delta^2\text{H}_{\text{Water}}$ , indicating a strong first-order control (Fig. S6). A simple isotope mass balance model (equation S1) suggests water contributes at least 56%  $\pm$  1% of the total H flux to lipids (Fig. S7). Further experimental work and complementary isotope flux models are needed to determine the specific pathways (and associated isotope effects) used during iGDGT synthesis in *S. acidocaldarius* (64).

Autotrophic archaea that produce iGDGTs, however, source their entire H budget to lipids from water in the growth environment and show more negative  $^{2}\epsilon_{L/W}$  values than those we observe for *S. acidocaldarius*. In the marine chemoautotroph, *N. maritimus*, grown in continuous culture, BP/water fractionation ranged from -272‰ to -260‰ (14). Similarly, BP/water fractionations for a metabolically flexible archaeon, *Archaeoglobus fulgidus*, ranged from -280‰ to -226‰ when cultured with several unique carbon substrates and electron donor/acceptor pairs (15). This difference may be driven by the distinct metabolic modes used (e.g., autotrophy vs heterotrophy) and/or by unique metabolic pathways that employ various intracellular hydride carriers and reductants to bring H's to the lipid sites, which could generate different net biosynthetic fractionations. Metabolic flux models suggest that in autotrophic archaea (e.g., *N. maritimus*), H-isotope

fractionation due to the electron transport chain and NADPH generation results in more depleted lipids than for heterotrophic archaea, such as *Sulfolobus* species because the source of NADPH impacts  ${}^2\varepsilon_{L/W}$  values (14). In both heterotrophic and aerobic archaea, most NADPH is generated by glucose dehydrogenase and potentially glyceraldehyde dehydrogenase from the Entner–Doudoroff pathway (73, 77).

Overall, the range of  ${}^2\varepsilon_{L/W}$  values in Archaeal lipids is narrower than the ranges observed in Bacteria or Eukarya (Fig. 6). While the sample size for Bacteria and Eukarya are twofold and fourfold larger than for Archaea, respectively, Bartlett's test for homogeneity of variances confirm that Archaeal  ${}^2\varepsilon_{L/W}$  values have smaller variance compared to Eukarya ( $K^2_{(1)} = 16.4, P < 0.0001$ ) and Bacteria ( $K^2_{(1)} = 118.5, P < 0.0001$ ) after accounting for sample size. Reported  ${}^2\varepsilon_{L/W}$  values for bacterial fatty acids vary over 600‰ and include large negative and large positive values (15, 33, 36, 38, 78). In Eukarya,  ${}^2\varepsilon_{L/W}$  values are uniformly negative and span over 300‰, though certain lipid classes group together (3, 25, 79). Lipids that are formed via the same biosynthetic pathway (e.g., acetogenic or isoprenoid pathway) tend to occupy distinct ranges of  ${}^2\varepsilon_{L/W}$  (15). Isoprenoid lipids produced via the MVA pathway in eukaryotes have similar  ${}^2\varepsilon_{L/W}$  values to iGDGT-derived biphytanes in archaea (15). This similarity suggests that the MVA pathway used for isoprenoid lipid biosynthesis has a large net fractionation in both domains of life.

## Applications and conclusion

Our calibration of biphytane  $\delta^2\text{H}$  composition as a proxy for the  $\delta^2\text{H}$  of environmental water in *S. acidocaldarius* has significant implications for paleohydroclimate and paleoecology reconstructions. First, this calibration may enable hydroclimate factors like precipitation, elevation, and seasonality to be reconstructed for environments that do not contain traditionally analyzed lipid biomarkers (e.g., plant waxes)—this includes extreme environments that do not support plant growth (e.g., terrestrial hydrothermal systems, salars, and hyperarid regions). Archaeal lipid  $\delta^2\text{H}$  values will be most powerful as a proxy in cases where a single-substrate source is a reasonable assumption.

Second, biphytane  $\delta^2\text{H}$  composition could be applied to marine or lacustrine sedimentary archives where multiple sources of organic matter are suspected, such as a mix of plant waxes representing *in situ* marine/aquatic production and allochthonous terrestrial production (e.g., aeolian deposition). In this case, plant wax  $\delta^2\text{H}$  values would reflect a mixture of growth waters (marine/lake water and soil water). In contrast, iGDGTs are likely derived solely from archaea living in the overlying water column with few potential terrestrial sources and thus the  $\delta^2\text{H}$  composition of iGDGTs would only reflect marine/lake water (42).

Here, we show that in the model thermoacidophile *S. acidocaldarius* grown on simple sugars, lipid-water fractionation ( ${}^2\varepsilon_{L/W}$ ) is not dependent on any of the environmental conditions tested or on growth rate. This finding suggests that *S. acidocaldarius* may have evolved stable metabolisms that exist in a constant NADPH deficit, possibly reflecting adaptation to energy-limiting environments. We conclude that *S. acidocaldarius* will likely demonstrate reliably invariant lipid/water fractionation regardless of growth rate, nutrient status, or energy availability, and that lipid/water fractionation may be more constant for certain archaeons than for phototrophic eukaryotes. For both domains, however, there is more variability in lipid/water fraction relative to the spatial and temporal variability in precipitation  $\delta^2\text{H}$  values, and more research is needed to understand the sources of this variation so that it can be accounted for in proxy applications.

This calibration underscores the potential for archaeal lipid  $\delta^2\text{H}$  composition as a proxy for past hydroclimates that could complement or be used independently of eukaryotic lipid  $\delta^2\text{H}$  composition. Future research should focus on exploring the effects of growth phase and metabolic pathways on lipid/water fractionation in *S. acidocaldarius* and other archaeal species. Expanding these investigations to include more diverse environmental conditions, such as varying carbon substrates or mixed microbial

communities, could further validate the consistency of  $^{2}\epsilon_{L/W}$  values and refine its utility as a hydrological proxy. Integrating isotope flux models with experimental data such as those generated here will allow us to better elucidate the specific biochemical pathways responsible for the observed fractionation patterns in domain Archaea.

## ACKNOWLEDGMENTS

This research was supported by research grant NSF EAR #1928303940 (W.D.L., S.K.); Simons Foundation Award #623881 (W.D.L.); Dartmouth College (W.D.L.); National Aeronautics and Space Administration (NASA) New Hampshire Space Grant (NASA-SSW-80NSSC19K0539); and Deutsche Forschungsgemeinschaft grant 441217575 (F.J.E.).

We thank the CU Boulder Earth Systems Stable Isotope Lab (CUBES-SIL) Core Facility (RRID:SCR\_019300) for analytical contributions; B. Chiu (then at Dartmouth), J. Blewett (then at Harvard), S. Carter (Harvard), and A. Maloney (CU Boulder) for expert laboratory support; Simon D. Kelly from International Atomic Energy Agency, Vienna, for measuring the  $\delta^{2}\text{H}$  composition of carbon substrates; and all members of the Leavitt lab for their support.

## AUTHOR AFFILIATIONS

<sup>1</sup>Department of Earth Sciences, Dartmouth College, Hanover, New Hampshire, USA

<sup>2</sup>Department of Geological Sciences, University of Colorado at Boulder, Boulder, Colorado, USA

<sup>3</sup>Department of Ecology, Evolution, and Marine Biology, U.C. Santa Barbara, Santa Barbara, California, USA

<sup>4</sup>Department of Earth & Planetary Sciences, Harvard University, Cambridge, Massachusetts, USA

<sup>5</sup>Leibniz-Laboratory for Radiometric Dating and Isotope Research, Kiel University, Kiel, Germany

<sup>6</sup>Department of Geology and Geophysics, University of Wyoming, Laramie, Wyoming, USA

<sup>7</sup>Department of Chemistry, Dartmouth College, Hanover, New Hampshire, USA

## PRESENT ADDRESS

Yuki Weber, Chroma Medicine, Boston, Massachusetts, USA

Yujiao Zhang, National Center for Science & Technology Evaluation, Beijing, China

Alice Zhou, Connecticut Agricultural Experiment Station, New Haven, Connecticut, USA

## AUTHOR ORCIDs

Carolynn M. Harris  <http://orcid.org/0000-0002-8254-556X>

Jeemin H. Rhim  <http://orcid.org/0000-0001-8129-0553>

Felix J. Elling  <http://orcid.org/0000-0003-0405-4033>

Alice Zhou  <http://orcid.org/0000-0001-5517-0865>

## FUNDING

Funder	Grant(s)	Author(s)
National Science Foundation (NSF)	1928303940	Sebastian Kopf William D. Leavitt
Simons Foundation (SF)	623881	William D. Leavitt
New Hampshire Space Grant	NASA-SSW-80NSSC19K0539	Carolynn M. Harris
Deutsche Forschungsgemeinschaft (DFG)	441217575	Felix J. Elling

## AUTHOR CONTRIBUTIONS

Carolynn M. Harris, Conceptualization, Data curation, Formal analysis, Investigation, Methodology, Project administration, Visualization, Writing – original draft, Writing – review and editing | Sebastian Kopf, Conceptualization, Data curation, Funding acquisition, Investigation, Writing – review and editing | Jeemin H. Rhim, Methodology, Writing – review and editing | Alec Cobban, Methodology, Writing – review and editing | Felix J. Elling, Data curation, Methodology, Writing – review and editing | Xiahong Feng, Methodology, Writing – review and editing | Jamie McFarlin, Methodology, Writing – review and editing | Yuki Weber, Methodology, Writing – review and editing | Yujiao Zhang, Data curation, Methodology, Writing – review and editing | Alice Zhou, Data curation, Methodology, Writing – review and editing | Harpreet Bather, Methodology, Writing – review and editing | Ann Pearson, Conceptualization, Funding acquisition, Methodology, Supervision, Writing – review and editing | William D. Leavitt, Conceptualization, Funding acquisition, Methodology, Supervision, Writing – review and editing

## ADDITIONAL FILES

The following material is available [online](#).

### Supplemental Material

**Supplemental material (AEM01983-24-s0001.docx).** Supplemental methods; Fig. S1 to S7.

**Table S1 (AEM01983-24-s0002.docx).** Summary of culture conditions and descriptive growth statistics for *S. acidocaldarius* grown in media prepared with <sup>2</sup>H-labeled waters. RPM refers to shaking rate.

**Table S2 (AEM01983-24-s0003.docx).** Descriptive statistics for individual biphytanyl (BP) lipids derived from iGDGTs for *S. acidocaldarius* grown in media prepared with <sup>2</sup>H-labeled waters.

## REFERENCES

- Gat JR. 1996. Oxygen and hydrogen isotopes in the hydrologic cycle. *Annu Rev Earth Planet Sci* 24:225–262. <https://doi.org/10.1146/annurev.earth.24.1.225>
- Hayes JM. 2001. Fractionation of carbon and hydrogen isotopes in biosynthetic processes. *Rev Mineral Geochem* 43:225–277. <https://doi.org/10.2138/gsmrg.43.1.225>
- Sessions AL, Burgoyne TW, Schimmelmann A, Hayes JM. 1999. Fractionation of hydrogen isotopes in lipid biosynthesis. *Org Geochem* 30:1193–1200. [https://doi.org/10.1016/S0146-6380\(99\)00094-7](https://doi.org/10.1016/S0146-6380(99)00094-7)
- Sessions AL, Sylva SP, Summons RE, Hayes JM. 2004. Isotopic exchange of carbon-bound hydrogen over geologic timescales. *Geochim Cosmochim Acta* 68:1545–1559. <https://doi.org/10.1016/j.gca.2003.06.004>
- Dawson D, Grice K, Wang SX, Alexander R, Radke J. 2004. Stable hydrogen isotopic composition of hydrocarbons in torbanites (Late Carboniferous to Late Permian) deposited under various climatic conditions. *Org Geochem* 35:189–197. <https://doi.org/10.1016/j.orggeochem.2003.09.004>
- Love GD, Zumbege JA. 2021. Emerging patterns in proterozoic lipid biomarker records. 1st ed. Cambridge University Press. <https://www.cambridge.org/core/product/identifier/9781108847117/type/element>.
- Liu J, An Z. 2019. Variations in hydrogen isotopic fractionation in higher plants and sediments across different latitudes: implications for paleohydrological reconstruction. *Sci Total Environ* 650:470–478. <https://doi.org/10.1016/j.scitotenv.2018.09.047>
- McFarlin JM, Axford Y, Masterson AL, Osburn MR. 2019. Calibration of modern sedimentary  $\delta^2\text{H}$  plant wax-water relationships in Greenland lakes. *Quat Sci Rev* 225:105978. <https://doi.org/10.1016/j.quascirev.2019.105978>
- Ladd SN, Nelson DB, Bamberger I, Daber LE, Kreuzwieser J, Kahmen A, Werner C. 2021. Metabolic exchange between pathways for isoprenoid synthesis and implications for biosynthetic hydrogen isotope fractionation. *New Phytol* 231:1708–1719. <https://doi.org/10.1111/nph.17510>
- Kaneko M, Kitajima F, Naraoka H. 2011. Stable hydrogen isotope measurement of archaeal ether-bound hydrocarbons. *Org Geochem* 42:166–172. <https://doi.org/10.1016/j.orggeochem.2010.11.002>
- Dirghangi SS, Pagani M. 2013. Hydrogen isotope fractionation during lipid biosynthesis by *Haloarcula marismortui*. *Geochim Cosmochim Acta* 119:381–390. <https://doi.org/10.1016/j.gca.2013.05.023>
- Lengger S, Weber Y, W. Taylor K, Kopf SH, Berstan R, D. Bull I, Maysr J-P, Leavitt WD, Blewett J, Pearson A, Pancost RD. 2020. Determination of the  $\delta^2\text{H}$  values of high molecular weight lipids by high temperature GC coupled to isotope ratio mass spectrometry. *Chemistry*. <https://doi.org/10.26434/chemrxiv.12668810.v1>
- Wu W, Meador TB, Könneke M, Elvert M, Wegener G, Hinrichs K-U. 2020. Substrate-dependent incorporation of carbon and hydrogen for lipid biosynthesis by *Methanosarcina barkeri*. *Environ Microbiol Rep* 12:555–567. <https://doi.org/10.1111/1758-2229.12876>
- Leavitt WD, Kopf SH, Weber Y, Chiu B, McFarlin JM, Elling FJ, Hoefft-McCann S, Pearson A. 2023. Controls on the hydrogen isotope composition of tetraether lipids in an autotrophic ammonia-oxidizing marine archaeon. *Geochim Cosmochim Acta* 352:194–210. <https://doi.org/10.1016/j.gca.2023.04.033>
- Rhim JH, Kopf S, McFarlin J, Maloney AE, Bather H, Harris CM, Zhou A, Feng X, Weber Y, Hoefft-McCann S, Pearson A, Leavitt WD. 2024. Metabolic imprints in the hydrogen isotopes of *Archaeoglobus fulgidus* tetraether lipids. *Geochim Cosmochim Acta* 386:196–212. <https://doi.org/10.1016/j.gca.2024.09.032>
- Sachs J. 2014. Hydrogen isotope signatures in the lipids of phytoplankton, p 79–94. In *Treatise on geochemistry*. Elsevier.
- Gao L, Edwards EJ, Zeng Y, Huang Y. 2014. Major evolutionary trends in hydrogen isotope fractionation of vascular plant leaf waxes. *PLoS One* 9:e112610. <https://doi.org/10.1371/journal.pone.0112610>
- Bender ALD, Suess M, Chitwood DH, Bradley AS. 2016. Investigating genetic loci that encode plant-derived paleoclimate proxies. *PP24B-03*

19. Baan J, Holloway-Phillips M, Nelson DB, Kahmen A. 2023. Species and biosynthetic effects cause uncorrelated variation in oxygen and hydrogen isotope compositions of plant organic compounds. *Geochim Cosmochim Acta* 352:1–13. <https://doi.org/10.1016/j.gca.2023.04.013>
20. Baan J. 2024. Understanding the metabolic signal in hydrogen isotope values of plant organic compounds. Thesis der Universität Basel <https://doi.org/10.5451/unibas-ep96717>
21. Ladd N, Nelson D, Matthews B, Dyer S, Limberger R, Klatt A, Narwani A, Dubois N, Schubert C. 2024. Taxon-specific hydrogen isotope signals in cultures and mesocosms facilitate ecosystem and hydroclimate reconstruction. *arXiv*. <https://doi.org/10.31223/X57T30>
22. Pilecky M, Kainz MJ, Wassenaar LI. 2024. Exploring hydrogen isotope fractionation in lipid biomolecules of freshwater algae: implications for ecological and paleoenvironmental studies. *Isotopes Environ Health Stud* 60:585–595. <https://doi.org/10.1080/10256016.2024.2419880>
23. Sachs JP, Kawka OE. 2015. The influence of growth rate on 2H/1H fractionation in continuous cultures of the coccolithophorid *Emiliana huxleyi* and the diatom *Thalassiosira pseudonana*. *PLoS One* 10:e0141643. <https://doi.org/10.1371/journal.pone.0141643>
24. van der Meer MTJ, Benthien A, French KL, Epping E, Zondervan I, Reichart G-J, Bijma J, Sinninghe Damsté JS, Schouten S. 2015. Large effect of irradiance on hydrogen isotope fractionation of alkenones in *Emiliana huxleyi*. *Geochim Cosmochim Acta* 160:16–24. <https://doi.org/10.1016/j.gca.2015.03.024>
25. Sachs JP, Maloney AE, Gregersen J, Paschall C. 2016. Effect of salinity on 2H/1H fractionation in lipids from continuous cultures of the coccolithophorid *Emiliana huxleyi*. *Geochim Cosmochim Acta* 189:96–109. <https://doi.org/10.1016/j.gca.2016.05.041>
26. Maloney AE, Shinneman ALC, Hemeon K, Sachs JP. 2016. Exploring lipid 2H/1H fractionation mechanisms in response to salinity with continuous cultures of the diatom *Thalassiosira pseudonana*. *Org Geochem* 101:154–165. <https://doi.org/10.1016/j.orggeochem.2016.08.015>
27. Wolfshorndl M, Danford R, Sachs JP. 2019. 2H/1H fractionation in microalgal lipids from the North Pacific Ocean: growth rate and irradiance effects. *Geochim Cosmochim Acta* 246:317–338. <https://doi.org/10.1016/j.gca.2018.11.027>
28. Torres-Romero I, Zhang H, Wijker RS, Clark AJ, McLeod RE, Jaggi M, Stoll HM. 2024. Hydrogen isotope fractionation is controlled by CO<sub>2</sub> in coccolithophore lipids. *Proc Natl Acad Sci U S A* 121:e2318570121. <https://doi.org/10.1073/pnas.2318570121>
29. Sachse D, Billault I, Bowen GJ, Chikaraishi Y, Dawson TE, Feakins SJ, Freeman KH, Magill CR, McInerney FA, van der Meer MTJ, Polissar P, Robins RJ, Sachs JP, Schmidt H-L, Sessions AL, White JWC, West JB, Kahmen A. 2012. Molecular paleohydrology: interpreting the hydrogen-isotopic composition of lipid biomarkers from photosynthesizing organisms. *Annu Rev Earth Planet Sci* 40:221–249. <https://doi.org/10.1146/annurev-earth-042711-105535>
30. Sessions AL. 2016. Factors controlling the deuterium contents of sedimentary hydrocarbons. *Org Geochem* 96:43–64. <https://doi.org/10.1016/j.orggeochem.2016.02.012>
31. Sessions AL, Jahnke LL, Schimmelmann A, Hayes JM. 2002. Hydrogen isotope fractionation in lipids of the methane-oxidizing bacterium *Methylococcus capsulatus*. *Geochim Cosmochim Acta* 66:3955–3969. [https://doi.org/10.1016/S0016-7037\(02\)00981-X](https://doi.org/10.1016/S0016-7037(02)00981-X)
32. Valentine DL. 2009. Isotopic remembrance of metabolism past. *Proc Natl Acad Sci U S A* 106:12565–12566. <https://doi.org/10.1073/pnas.0906428106>
33. Zhang X, Gillespie AL, Sessions AL. 2009. Large D/H variations in bacterial lipids reflect central metabolic pathways. *Proc Natl Acad Sci USA* 106:12580–12586. <https://doi.org/10.1073/pnas.0903030106>
34. Dawson KS, Osburn MR, Sessions AL, Orphan VJ. 2015. Metabolic associations with archaea drive shifts in hydrogen isotope fractionation in sulfate-reducing bacterial lipids in cocultures and methane seeps. *Geobiology* 13:462–477. <https://doi.org/10.1111/gbi.12140>
35. Leavitt WD. 2016. The inner lives of archaea: the hydrogen isotopic composition of Archaeal lipids as a proxy of metabolic state
36. Osburn MR, Dawson KS, Fogel ML, Sessions AL. 2016. Fractionation of hydrogen isotopes by sulfate- and nitrate-reducing bacteria. *Front Microbiol* 7:1166. <https://doi.org/10.3389/fmicb.2016.01166>
37. Leavitt WD, Murphy SJ, Lynd LR, Bradley AS. 2017. Hydrogen isotope composition of *Thermoanaerobacterium saccharolyticum* lipids: comparing wild type with a nfn-transhydrogenase mutant. *Org Geochem* 113:239–241. <https://doi.org/10.1016/j.orggeochem.2017.06.020>
38. Wijker RS, Sessions AL, Fuhrer T, Phan M. 2019. <sup>2</sup>H/<sup>1</sup>H variation in microbial lipids is controlled by NADPH metabolism. *Proc Natl Acad Sci U S A* 116:12173–12182. <https://doi.org/10.1073/pnas.1818372116>
39. van de Vossenberg JLCM, Driessen AJM, Konings WN. 1998. The essence of being extremophilic: the role of the unique archaeal membrane lipids. *Extremophiles* 2:163–170. <https://doi.org/10.1007/s007920050056>
40. Schouten S, Hopmans EC, Sinninghe Damsté JS. 2013. The organic geochemistry of glycerol dialkyl glycerol tetraether lipids: a review. *Org Geochem* 54:19–61. <https://doi.org/10.1016/j.orggeochem.2012.09.006>
41. Schouten S, Hopmans EC, Schefuß E, Sinninghe Damsté JS. 2002. Distributional variations in marine crenarchaeal membrane lipids: a new tool for reconstructing ancient sea water temperatures? *Earth Planet Sci Lett* 204:265–274. [https://doi.org/10.1016/S0012-821X\(02\)00979-2](https://doi.org/10.1016/S0012-821X(02)00979-2)
42. Pearson A, Ingalls AE. 2013. Assessing the use of archaeal lipids as marine environmental proxies. *Annu Rev Earth Planet Sci* 41:359–384. <https://doi.org/10.1146/annurev-earth-050212-123947>
43. De Rosa M, Gambacorta A. 1988. The lipids of archaeobacteria. *Prog Lipid Res* 27:153–175. [https://doi.org/10.1016/0163-7827\(88\)90011-2](https://doi.org/10.1016/0163-7827(88)90011-2)
44. Elling FJ, Könneke M, Lipp JS, Becker KW, Gagen EJ, Hinrichs K-U. 2014. Effects of growth phase on the membrane lipid composition of the thaumarchaeon *Nitrosopumilus maritimus* and their implications for archaeal lipid distributions in the marine environment. *Geochim Cosmochim Acta* 141:579–597. <https://doi.org/10.1016/j.gca.2014.07.005>
45. Elling FJ, Könneke M, Nicol GW, Stieglmeier M, Bayer B, Spieck E, de la Torre JR, Becker KW, Thomm M, Prosser JI, Herndl GJ, Schleper C, Hinrichs K. 2017. Chemotaxonomic characterisation of the thaumarchaeal lipidome. *Environ Microbiol* 19:2681–2700. <https://doi.org/10.1111/1462-2920.13759>
46. Hurley SJ, Elling FJ, Könneke M, Buchwald C, Wankel SD, Santoro AE, Lipp JS, Hinrichs KU, Pearson A. 2016. Influence of ammonia oxidation rate on thaumarchaeal lipid composition and the TEX<sub>86</sub> temperature proxy. *Proc Natl Acad Sci USA* 113:7762–7767. <https://doi.org/10.1073/pnas.1518534113>
47. Cobban A, Zhang Y, Zhou A, Weber Y, Elling FJ, Pearson A, Leavitt WD. 2020. Multiple environmental parameters impact lipid cyclization in *Sulfolobus acidocaldarius*. *Environ Microbiol* 22:4046–4056. <https://doi.org/10.1111/1462-2920.15194>
48. Zhou A, Weber Y, Chiu BK, Elling FJ, Cobban AB, Pearson A, Leavitt WD. 2020. Energy flux controls tetraether lipid cyclization in *Sulfolobus acidocaldarius*. *Environ Microbiol* 22:343–353. <https://doi.org/10.1111/1462-2920.14851>
49. Quehenberger J, Pittenauer E, Allmaier G, Spadiut O. 2020. The influence of the specific growth rate on the lipid composition of *Sulfolobus acidocaldarius*. *Extremophiles* 24:413–420. <https://doi.org/10.1007/s00792-020-01165-1>
50. Yang W, Chen H, Chen Y, Chen A, Feng X, Zhao B, Zheng F, Fang H, Zhang C, Zeng Z. 2023. Thermophilic archaeon orchestrates temporal expression of GDGT ring synthases in response to temperature and acidity stress. *Environ Microbiol* 25:575–587. <https://doi.org/10.1111/1462-2920.16301>
51. Brock TD, Brock KM, Belly RT, Weiss RL. 1972. *Sulfolobus*: a new genus of sulfur-oxidizing bacteria living at low pH and high temperature. *Archiv Mikrobiol* 84:54–68. <https://doi.org/10.1007/BF00408082>
52. Bischof LF, Haurat MF, Hoffmann L, Albersmeier A, Wolf J, Neu A, Pham TK, Albaum SP, Jakobi T, Schouten S, Neumann-Schaal M, Wright PC, Kalinowski J, Siebers B, Albers S-V. 2018. Early response of *Sulfolobus acidocaldarius* to nutrient limitation. *Front Microbiol* 9:3201. <https://doi.org/10.3389/fmicb.2018.03201>
53. Quehenberger J, Shen L, Albers S-V, Siebers B, Spadiut O. 2017. *Sulfolobus* - a potential key organism in future biotechnology. *Front Microbiol* 8:2474. <https://doi.org/10.3389/fmicb.2017.02474>
54. Boyd ES, Pearson A, Pi Y, Li W-J, Zhang YG, He L, Zhang CL, Geesey GG. 2011. Temperature and pH controls on glycerol dibiphytanyl glycerol tetraether lipid composition in the hyperthermophilic crenarchaeon *Acidilobus sulfurireducens*. *Extremophiles* 15:59–65. <https://doi.org/10.1007/s00792-010-0339-y>
55. Jensen SM, Brandl M, Treusch AH, Ejsing CS. 2015. Structural characterization of ether lipids from the archaeon *Sulfolobus islandicus* by high-resolution shotgun lipidomics. *J Mass Spectrom* 50:476–487. <https://doi.org/10.1002/jms.3553>
56. Wagner M, van Wolferen M, Wagner A, Lassak K, Meyer BH, Reimann J, Albers S-V. 2012. Versatile genetic tool box for the crenarchaeote

- Sulfolobus acidocaldarius*. Front Microbiol 3. <https://doi.org/10.3389/fmicb.2012.00214>
57. Zhang YG, Pagani M, Wang Z. 2016. Ring index: a new strategy to evaluate the integrity of TEX<sub>86</sub> paleothermometry. Paleogeography 31:220–232. <https://doi.org/10.1002/2015PA002848>
58. Abraham A, Cannavan A, Kelly SD. 2020. Stable isotope analysis of non-exchangeable hydrogen in carbohydrates derivatised with N-methyl-bis-trifluoroacetamide by gas chromatography - Chromium silver reduction/High temperature Conversion-isotope ratio mass spectrometry (GC-CrAg/HTC-IRMS). Food Chem 318:126413. <https://doi.org/10.1016/j.foodchem.2020.126413>
59. Kopf S, Davidheiser-Kroll B, Kocken I. 2021. Isoreader: an R package to read stable isotope data files for reproducible research. JOSS 6:2878. <https://doi.org/10.21105/joss.02878>
60. Harris C. 2025. Carolyneharris/Saci\_Enviro\_d2H: Supplementary material for Harris et al., 2025, AEM (v.1.0.1). <https://doi.org/10.5281/zenodo.14743997>
61. Lewis AM, Recalde A, Bräsen C, Counts JA, Nussbaum P, Bost J, Schocke L, Shen L, Willard DJ, Quax TEF, Peeters E, Siebers B, Albers S-V, Kelly RM. 2021. The biology of thermoacidophilic archaea from the order *Sulfolobales*. FEMS Microbiol Rev 45:1–60. <https://doi.org/10.1093/femsr/efuaa063>
62. Reysenbach A-L, Cady SL. 2001. Microbiology of ancient and modern hydrothermal systems. Trends Microbiol 9:79–86. [https://doi.org/10.1016/S0966-842X\(00\)01921-1](https://doi.org/10.1016/S0966-842X(00)01921-1)
63. Auernik KS, Cooper CR, Kelly RM. 2008. Life in hot acid: pathway analyses in extremely thermoacidophilic archaea. Curr Opin Biotechnol 19:445–453. <https://doi.org/10.1016/j.copbio.2008.08.001>
64. Harris C, Rhim J, Zhang Y, Cobban A, McFarlin J, Batther H, Kopf S, Leavitt W. 2022. Determining controls on hydrogen isotope fractionation in archaeal tetraether lipids in a thermoacidophilic archaeal heterotroph. Goldschmidt2022 Abstracts. European Association of Geochemistry, Honolulu, HI, USA.
65. Siliakus MF, van der Oost J, Kengen SWM. 2017. Adaptations of archaeal and bacterial membranes to variations in temperature, pH and pressure. Extremophiles 21:651–670. <https://doi.org/10.1007/s00792-017-0939-x>
66. Jia B, Liu J, Van Duyet L, Sun Y, Xuan YH, Cheong G-W. 2015. Proteome profiling of heat, oxidative, and salt stress responses in *Thermococcus kodakarensis* KOD1. Front Microbiol 6. <https://doi.org/10.3389/fmicb.2015.00605>
67. Sachs JP, Schwab VF. 2011. Hydrogen isotopes in dinosterol from the Chesapeake Bay estuary. Geochim Cosmochim Acta 75:444–459. <https://doi.org/10.1016/j.gca.2010.10.013>
68. Thauer RK, Kaster A-K, Seedorf H, Buckel W, Hedderich R. 2008. Methanogenic archaea: ecologically relevant differences in energy conservation. Nat Rev Microbiol 6:579–591. <https://doi.org/10.1038/nrmicro1931>
69. Spaans SK, Weusthuis RA, van der Oost J, Kengen SWM. 2015. NADPH-generating systems in bacteria and archaea. Front Microbiol 6:742. <https://doi.org/10.3389/fmicb.2015.00742>
70. Wakagi T, Oshima T. 1987. Energy metabolism of a thermoacidophilic archaeobacterium, *Sulfolobus acidocaldarius*. Origins Life Evol Biosphere 17:391–399. <https://doi.org/10.1007/BF02386477>
71. Liu L-J, Jiang Z, Wang P, Qin Y-L, Xu W, Wang Y, Liu S-J, Jiang C-Y. 2021. Physiology, taxonomy, and sulfur metabolism of the Sulfolobales, an order of thermoacidophilic archaea. Front Microbiol 12:768283. <https://doi.org/10.3389/fmicb.2021.768283>
72. Valentine DL. 2007. Adaptations to energy stress dictate the ecology and evolution of the Archaea. Nat Rev Microbiol 5:316–323. <https://doi.org/10.1038/nrmicro1619>
73. Bräsen C, Esser D, Rauch B, Siebers B. 2014. Carbohydrate metabolism in Archaea: current insights into unusual enzymes and pathways and their regulation. Microbiol Mol Biol Rev 78:89–175. <https://doi.org/10.1128/MBR.00041-13>
74. Schouten S, Ossebaer J, Schreiber K, Kienhuis MVM, Langer G, Benthien A, Bijma J. 2006. The effect of temperature, salinity and growth rate on the stable hydrogen isotopic composition of long chain alkenones produced by *Emiliania huxleyi* and *Gephyrocapsa oceanica*. Biogeosciences 3:113–119. <https://doi.org/10.5194/bg-3-113-2006>
75. Zhang Z, Sachs JP, Marchetti A. 2009. Hydrogen isotope fractionation in freshwater and marine algae: II. Temperature and nitrogen limited growth rate effects. Org Geochem 40:428–439. <https://doi.org/10.1016/j.orggeochem.2008.11.002>
76. Quehenberger J, Albersmeier A, Glatzel H, Hackl M, Kalinowski J, Spadiut O. 2019. A defined cultivation medium for *Sulfolobus acidocaldarius*. J Biotechnol 301:56–67. <https://doi.org/10.1016/j.jbiotec.2019.04.028>
77. Nunn CEM, Johnsen U, Schönheit P, Fuhrer T, Sauer U, Hough DW, Danson MJ. 2010. Metabolism of pentose sugars in the hyperthermophilic archaea *Sulfolobus solfataricus* and *Sulfolobus acidocaldarius*. J Biol Chem 285:33701–33709. <https://doi.org/10.1074/jbc.M110.146332>
78. Campbell BJ, Li C, Sessions AL, Valentine DL. 2009. Hydrogen isotopic fractionation in lipid biosynthesis by H<sub>2</sub>-consuming *Desulfobacterium autotrophicum*. Geochim Cosmochim Acta 73:2744–2757. <https://doi.org/10.1016/j.gca.2009.02.034>
79. Zhang Z, Sachs JP. 2007. Hydrogen isotope fractionation in freshwater algae: I. Variations among lipids and species. Org Geochem 38:582–608. <https://doi.org/10.1016/j.orggeochem.2006.12.004>